Terahertz Reflectarrays and Nonuniform Metasurfaces

Daniel Headland, *Member, IEEE*, Tiaoming Niu, Eduardo Carrasco, *Member, IEEE*, Derek Abbott, *Fellow, IEEE*, Sharath Sriram, *Member, IEEE*, Madhu Bhaskaran, *Member, IEEE*, Christophe Fumeaux, *Senior Member, IEEE*, and Withawat Withayachumnankul, *Senior Member, IEEE*

(Invited Paper)

***Abstract*—This paper covers our recent work on terahertz reflectarray antennas, providing a broad, critical perspective, and contrasting different approaches. The reflectarray antenna is a well-established device that offers significant control and freedom over the directionality and characteristics of its radiation pattern. Such a capability is critical to the successful development of commercially viable terahertz technologies. In this paper, the design, fabrication, and experimental characterization of four terahertz reflectarray devices is presented, based on two different classes of terahertz resonator. The first class is the metallic resonator, and three such reflectarray devices are presented, with each offering its own particular birefringent behavior. The second class is the dielectric resonator, which promises higher efficiency than the metallic resonator, and one such reflectarray device is presented. Devices such as these provide significant design freedom for defining particular beam-shaping operations for diverse application requirements. It is hoped that, with future advances in terahertz resonator technology, reflectarray antennas will prove instrumental in facilitating numerous promising applications of the terahertz range, including high-volume communications, noninvasive medical imaging, and security screening.**

***Index Terms*—Terahertz, reflectarray, metallic patch resonator antenna, dielectric resonator antenna, wavefront engineering, metasurface.**

I. Introduction

THE terahertz range has been identified as possessing significant potential for applications including high-volume wireless communications over short distances [1]–[3], noninvasive medical imaging [4], [5], and non-destructive security screening [6]. However, the commercial deployment of such technologies has been limited by practical challenges. These issues include long-standing difficulties in generating significant terahertz power with compact sources due to a lack of mature components and systems [7], [8], and high attenuation in typical atmospheric conditions [9]. Both of these factors contribute to degradation in signal quality. Thus, in order to maintain an adequate signal-to-noise ratio, practical terahertz systems must waste as little radiated terahertz power as possible.

Beam control techniques can be used to increase antenna directivity, which is in support of the aforementioned goal of avoiding inefficiency, provided correct alignment is observed. This is particularly relevant for higher frequencies, as a shorter wavelength results in a lower effective antenna aperture, and hence lower collected power, for a given value of antenna gain. Beam control techniques will therefore be necessary for the deployment of terahertz technologies, in order to minimize the amount of power that is not directed at the receiver. Such techniques can also be employed to achieve customizable radiation pattern characteristics such as shaped beams, polarization diversity, or sidelobe suppression. Lastly, dynamic beam control can be used to steer the direction of the radiation maximum, to maintain alignment and connectivity between high-gain transceivers without the need for manual realignment. Given the particular characteristics of radiation in the millimeter-wave range and above, such dynamic beam control technology is likely to be necessary, even with the most optimistic projections of advances in terahertz output power capability [3].

One of the most prolific and popular approaches to beam control is the reflectarray antenna [10], which is deployed in conjunction with a feed antenna, and manipulates radiation upon reflection. Such a device typically consists of a planar array of subwavelength-sized passive antennas, which are also known as resonators in this context. It is also worth mentioning that resonators are not the only available choice for this purpose; true-time delays have also been widely implemented in planar reflectarrays [11], [12]. The elements of this array individually interact with locally-incident radiation, and they collectively alter the characteristics of the overall reflected radiation pattern in accordance with the well-understood principles of array theory. In general, such a device offers versatility, customizability, efficiency, possible birefringence, and simplicity. In contrast

Manuscript received October 4, 2016; revised December 12, 2016; accepted December 13, 2016.

D. Headland, D. Abbott, C. Fumeaux, and W. Withayachumnankul are with the School of Electrical and Electronic Engineering, The University of Adelaide, Adelaide, SA 5005, Australia (e-mail: daniel.headland@adelaide.edu.au; derek.abbott@adelaide.edu.au; christophe.fumeaux@adelaide.edu.au; withawat@eleceng.adelaide.edu.au).

T. Niu is with the Applied Technology Engineering Research Center, Lanzhou University, Lanzhou 730000, China (e-mail: niutm@lzu.edu.cn).

E. Carrasco is with the Foundation for Research on Information Technologies in Society, IT'IS, Zurich 8004, Switzerland (e-mail: carrasco@itis.ethz.ch).

S. Sriram and M. Bhaskaran are with the Functional Materials and Microsystems Group, and the MicroNano Research Facility, RMIT University, Melbourne, VIC 3000, Australia (e-mail: sharath.sriram@gmail.com; madhu.bhaskaran@gmail.com).

Color versions of one or more of the figures in this paper are available online at http://ieeexplore.ieee.org.

Digital Object Identifier 10.1109/JSTQE.2016.2640452

to beam control techniques such as phased array antennas, a reflectarray is fed from free-space, which eliminates the need for a feed network to drive the individual array elements. This is beneficial to terahertz applications, as a feed network is often lossy and complicated, particularly at higher frequencies, which places practical limitations on the achievable size of the overall array.

The reflectarray concept was originally conceived of in the microwave range in the early 1960's, in the form of a bulky array of shorted waveguides of various lengths [13]. This design was proposed as a versatile alternative to physically-shaped reflectors, providing far greater control over radiation characteristics. Subsequently, the development of reflectarrays was accelerated by the advent of printable microstrip antenna technology, as it enabled individual resonator elements to be made planar and compact [14], [15]. For the first few decades following their inception, the development of reflectarray antennas remained limited to the the microwave range exclusively. However, more recently the concept has seen adoption in other frequency ranges such as the optical [16]–[19], and terahertz ranges [20], which illustrates their true scope across the electromagnetic spectrum.

The reflectarray antenna is related to the concept of a transmitarray [21], in that both employ passive resonators in conjunction with array theory to achieve beam control. The difference is that, for a transmitarray, radiation is transmitted through the device rather than reflected from it. There is a trade-off between these two approaches. A transmitarray is generally less efficient due to factors involving reflection loss, and the need for either multi-layer configurations [22] or polarization converter-based designs [23]. On the other hand, a reflectarray has complications associated with feed blockage. For the purposes of this article, we will focus on reflectarrays over transmitarrays. Our choice in this matter is informed by a desire to maintain efficiency, due to the aforementioned power-related constraints in the terahertz range.

Each of these array-antenna devices can be thought of more generally as an electrically large array of sub-wavelength scattering elements, in which the local interaction of individual elements with electromagnetic waves collectively results in some overall desirable behavior. Thus, this larger family of devices includes metamaterials [24]–[26], and their planar counterpart, metasurfaces [27], [28]. In the last few years there have been numerous examples in the literature of nonuniform metasurfaces, for beam control either in transmission or reflection [29], [30]. The operation of such devices is described by generalized Snell's law, which incorporates a phase discontinuity at the interface [31], [32]. Despite that, nonuniform metasurfaces of this sort can validly be referred to as reflectarrays and transmitarrays [33], and the generalized form of Snell's law reconciles well with array theory in the microwave range, and with diffraction in the optical range [34].

Nevertheless, terahertz reflectarrays can benefit from both the array theory and metasurface paradigms, and can draw on optical and microwave technologies alike for inspiration. However, the practical challenges and application requirements encountered in each of these frequency ranges are unique. Firstly, the scale of a terahertz wavelength is in the order of hundreds of micrometers. As such, microfabrication techniques are available that provide more freedom than the nanofabrication techniques that are necessary in the optical range. On the other hand, the larger scale of devices in the microwave range provides greater freedom still, making it possible to incorporate vias, off-chip devices, and complicated topologies that are not feasible to realize in the terahertz range [35]. Furthermore, there is less choice in the materials available in the terahertz range, owing to an absence of natural materials that exhibit a strong interaction with terahertz radiation. Additionally, due to the lack of available power in the terahertz range, efficiency is a key concern in the design of terahertz devices. Lastly, the terahertz range is lacking in electronically-tunable devices that can feasibly be incorporated into reflectarray and metasurface designs, and this has significantly hindered the development of reconfigurable terahertz reflectarrays. That said, important efforts are underway to incorporate novel materials such as liquid crystals [36] or graphene [37].

Aside from array antennas and metasurfaces, there are other approaches to achieving beam control in the terahertz range that are worthy of mention. Firstly, a laboratory environment will most often make use of geometric optics, including lenses and parabolic reflectors, as such devices are mature and offer low dispersion, as well as high bandwidth and efficiency. However, practical applications demand a higher degree of compactness than laboratory systems, and hence flat-profile devices are preferable. Another approach is the use of diffractive optics, which makes use of a low-profile topology to manipulate radiation, as opposed to arrayed subwavelength structures [38], [39]. Such devices promise high efficiency, but cannot offer the same versatility and potential for birefringence of reflectarrays. As such, reflectarrays are the focus of this work.

This article summarizes some of our recent work on terahertz reflectarray antennas. We present theoretical background in Section II, relevant fabrication methodologies in Section III, our work on metallic resonator-based reflectarrays in Section IV [40]–[42], and our work on dielectric resonator-based reflectarrays in Section V [43]. Lastly, Section VI gives some insight into how research effort in this field could best be utilized, given certain key obstacles, and Section VII provides a conclusion. Note all reflectarray antennas presented in the present work are designed to operate in the vicinity of 1 THz, as this is identified as most representative of the terahertz range as a whole. Despite this, the structures are readily scalable within the terahertz range in order to meet the particular requirements of specific applications.

II. Reflectarray Antennas

This section gives a concise summary of aspects of reflectarray antenna theory and design that are relevant to the terahertz range. Reflectarray design is performed at two levels. The required discrete phase distribution for a given beam control operation must be determined, as briefly discussed in Section II-A. In order to achieve this phase distribution, a suitable physical realization of a resonator must be selected to tune the phase response, as discussed in Section II-B. These

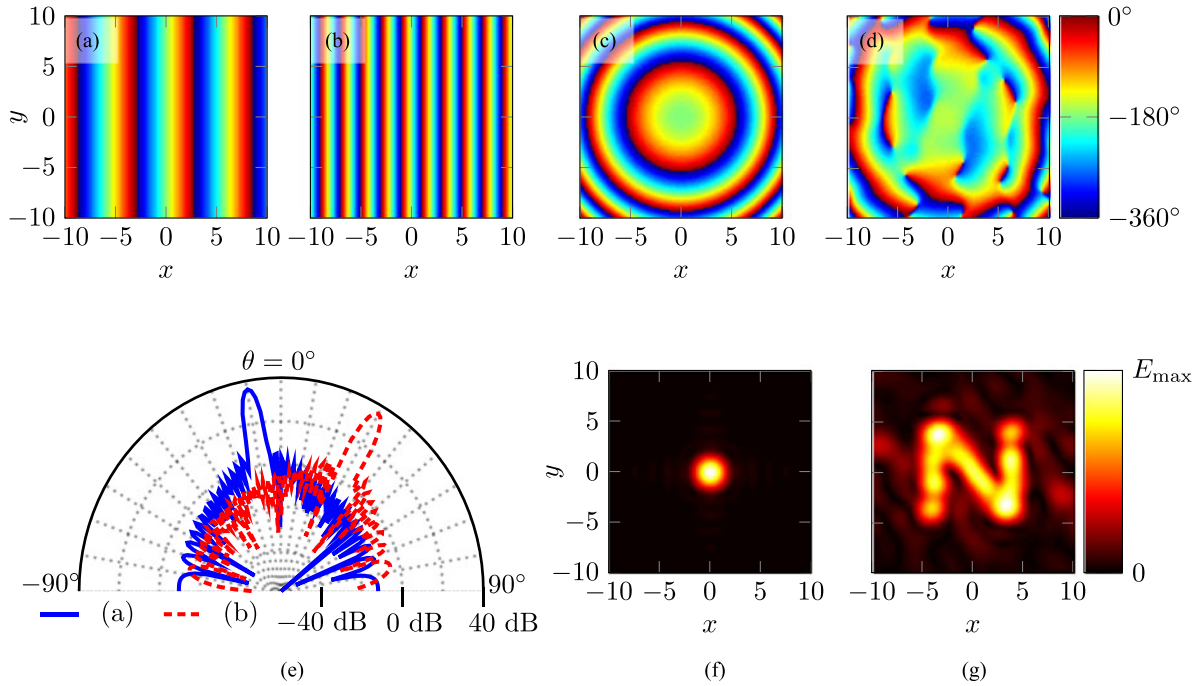

Fig. 1. Illustration of the principles of wavefront engineering, showing (a-d) phase distributions required to produce various beam control operations. Phase distributions (a) and (b) produce far-field beam steering shown in (e), phase distribution (c) produces the focal spot shown in (f), and phase distribution (d) produces a Gerchberg-Saxton hologram, representing the letter capital "N", in (g). All spatial dimensions are in units of wavelength, for generality. The propagation distance in both (f) and (g) is 30λ. In all cases, a 15λ-diameter Gaussian magnitude profile is employed in order to suppress sidelobes and fringing effects.

concerns are certainly inter-related, but it is useful to consider them as being conceptually independent.

A. *Wavefront Engineering*

Broadly speaking, wavefront engineering can be considered the manipulation of the field distribution across a given aperture in order to achieve some desired near- or far-field radiation characteristics. In order to illustrate this concept, we will assume that the incident field distribution is of constant phase profile. Additionally, we will consider the field distribution of the output wavefront abstractedly, without stating the mechanism by which a required field distribution is achieved. When defining a given field distribution there are two spatially-dependent parameters to consider, which are amplitude and phase. Both can be employed to manipulate the propagating behavior of a wave, but we will focus on phase-based techniques in the present work, as phase control provides greater versatility, more control over beam characteristics, and higher efficiency in terms of both aperture and radiation efficiency.

For a linear phased array antenna, a progressive phase difference between regularly-spaced elements results in beam steering off to a non-normal angle in the far field [44]. Phenomenologically, this can be explained with the retardation of the wavefront on one side of the array with respect to the other, resulting in a tilt of the subsequent wavefront, and hence in steering of the propagating wave. A planar array of radiators possessing progressive phase can be considered conceptually equivalent to a wavefront with a (stair-cased) linear-ramp phase distribution. In order to achieve steering towards angle θ_s with respect to the normal in the xz-plane, the following phase distribution is required across the surface in the xy-plane,

$$\varphi(x, y) = k_0 x \sin(-\theta_s), \tag{1}$$

where k_0 is the free-space wavenumber. Note that phase is wrapped to a 360° cycle, which effectively translates the ramp into a sawtooth function, as shown in Figs. 1(a,b). This is similar to conventional blazed diffraction gratings. The phase distribution shown is discretized with a step size of $\lambda/5$, to represent the finite number of resonators used in practical cases. The array factor (AF), i.e. the far-field radiation pattern for isotropic sources, is computed on the basis of array theory using the following expression,

$$\mathrm{AF}(\theta, \phi) = \sum_{n=1}^{N} A_n \exp\left(jk_0(x_n \sin\theta\cos\phi + y_n \sin\theta \sin\phi)\right), \tag{2}$$

in which A_n is the complex amplitude of the nth element,

$$A_n = a_n \exp\left(j\varphi_n\right), \tag{3}$$

where a_n is scalar field magnitude, and φ_n corresponds to the phase distribution in (1), substituting x_n for x. Thus, the array factor sums the radiation of all elements accounting for their phase, φ_n, and path difference. The resulting radiation patterns are shown in Fig. 1(e), where it is noted that a Gaussian beam excitation provides a low-sidelobe illumination. In practical cases, the overall radiation pattern is computed by taking the product of the array factor and the element's radiation pattern, but the array factor in isolation is generally sufficient to illustrate the beam-shaping operation. It can be seen that the direction and

gradient of the phase ramp determine the angle of the far-field radiation pattern maximum. More generally, shaped beams are achievable with similar techniques [45], [46], providing highly customizable far-field radiation patterns. For example, satellite communications employ such techniques in order to define a specific beam shape that corresponds to the contour of the geographical region to be serviced, and this minimizes the amount of power projected outside the bounds of the relevant region [47]–[49].

Additional to beam steering and other far-field beam control techniques, wavefront engineering of this sort can be employed in order to achieve or approximate a desired field magnitude distribution at a given finite propagation distance. The most common example of an operation such as this is focusing, in which the resultant beam converges to a focal point at a finite distance. This is achieved by imposing a spherical phase distribution on a propagating wavefront, to ensure that all paths from the wavefront to focal point have the same effective phase retardation. The phase distribution on the surface required to achieve this operation is as follows,

$$\varphi(x,y) = k_0\left(\sqrt{F^2+(x^2+y^2)}-F\right)+\varphi_0, \tag{4}$$

for a given focal length F, with some arbitrary initial phase φ_0. An example of such a phase distribution is illustrated in Fig. 1(c), and the resultant field distribution is shown in Fig. 1(f). This field distribution is approximately calculated using scalar diffraction theory [50], which takes the following Riemann-sum form for discretized field distributions,

$$A(x,y,z) = \frac{1}{j\lambda}\sum_{n=1}^{N} A^*(x_n,y_n,0)\frac{\exp(jk_0r_{01})\cos\theta_{01}}{r_{01}}\Delta x\Delta y, \tag{5}$$

where Δx and Δy describe element-spacing, $r_{01} = \sqrt{(x-x_n)^2+(y-y_n)^2+z^2}$ is the length of a line segment connecting a point in one plane, (x,y,z), to a point on the initial wavefront, $(x_n,y_n,0)$, and θ_{01} is the angle made between this line segment and the z-axis. The variable $A(x_n,y_n,0)$ is the complex field amplitude, which in this case can be computed by substituting the expression for φ_n given in (4) into (3). Note that, in practical reflectarray applications, such devices are most commonly deployed in a reciprocal arrangement, in which the feed antenna is placed at the focal point. This allows the reflectarray to transform divergent, spherical wavefronts into planar wavefronts, and hence increases the gain of a transmitting antenna.

More generally, with techniques such as the Gerchberg-Saxton phase retrieval algorithm [51], it is possible to specify a near-arbitrary field amplitude distribution, and calculate the phase distribution required to produce it at a given propagation distance. To illustrate this concept, the phase distribution given in Fig. 1(d) is calculated using a variant of the Gerchberg-Saxton phase retrieval algorithm that uses scalar diffraction theory rather than the two-dimensional fast Fourier transform. For this example, the required output field distribution is a representation of the capital letter "N". Scalar diffraction theory is also employed to determine its output field distribution, and this is shown in Fig. 1(g). It is clearly visible that the bespoke capital letter has been reproduced with adequate fidelity.

B. Reflective Resonator

An infinite array of identical, single-mode reflective resonators that interacts with incident free-space fields can be modeled as a one-port network with complex reflection coefficient Γ. This implies that all of the energy reflected from the array is scattered in the specular direction, which is only valid if the periodicity is subwavelength. If, on the other hand, the inter-element spacing is greater than or equal to a wavelength, then energy will be diffracted into grating lobes [44]. This is because the array effectively behaves as a diffraction grating, and hence it scatters radiation into multiple directions, as dictated by its periodicity. In some cases, the use of inter-element spacings of less than a sixth of a wavelength is advocated, in order to achieve a smoother phase gradient [22], [52]. In practice, however, a half-wavelength spacing is sufficient for most applications. Such larger inter-element spacings will in-general provide a larger phase tunability range, and hence an inter-element spacing close to this value is adopted for all of the devices demonstrated in the present work.

In order to explore the connection between passive resonators and phase control, the following expression for the reflection coefficient of a resonator is employed [53],

$$\Gamma = -1 + \frac{2\pi f_0 Q_{\mathrm{a}}}{\frac{Q_{\mathrm{a}}}{2}+\frac{Q_{\mathrm{r}}}{2}-jQ_{\mathrm{r}}Q_{\mathrm{a}}\left(\frac{f}{f_0}-1\right)}. \tag{6}$$

This models a resonator with a single mode of resonance, which is described by the resonance frequency f_0, the radiation quality factor Q_{r}, and the absorption quality factor Q_{a}. The latter two quantities relate to energy exchanged with free space and energy lost to dissipation respectively. For devices relevant to the present work, the condition $Q_{\mathrm{a}} \gg Q_{\mathrm{r}}$ is assumed, which describes efficient resonators with a large phase tunability range. An ideal case of this, in which no energy is dissipated, is presented in Fig. 2(a). This shows very clearly that, on-resonance, the response is purely real, and reflection phase is 0°. As such, the reflection response at the resonance frequency is identical to that of a perfect magnetic conductor (PMC), and hence a resonator of this sort can be considered to exhibit a magnetic response. By contrast, a perfect electrical conductor (PEC) also exhibits purely real reflection response, but the reflection phase is $\pm 180^\circ$. Whilst a resonator of this sort exhibits a magnetic response on-resonance, it approaches an electrical response away from resonance, heading towards $+180^\circ$ as $f \to 0$, and -180° as $f \to \infty$. Thus, if the frequency of operation, f, is gradually detuned from the resonance frequency, f_0, the resonator can cover a range of reflection phase close to 360°. As such, the operation of a given reflectarray antenna hinges on the capacity to tune the resonance frequency, f_0, of a passive resonator away from the operating frequency of f. In the present work, this is achieved by varying the geometry of a given resonator, but it is also possible to tune a reflective resonator electronically, at least in the microwave range [54].

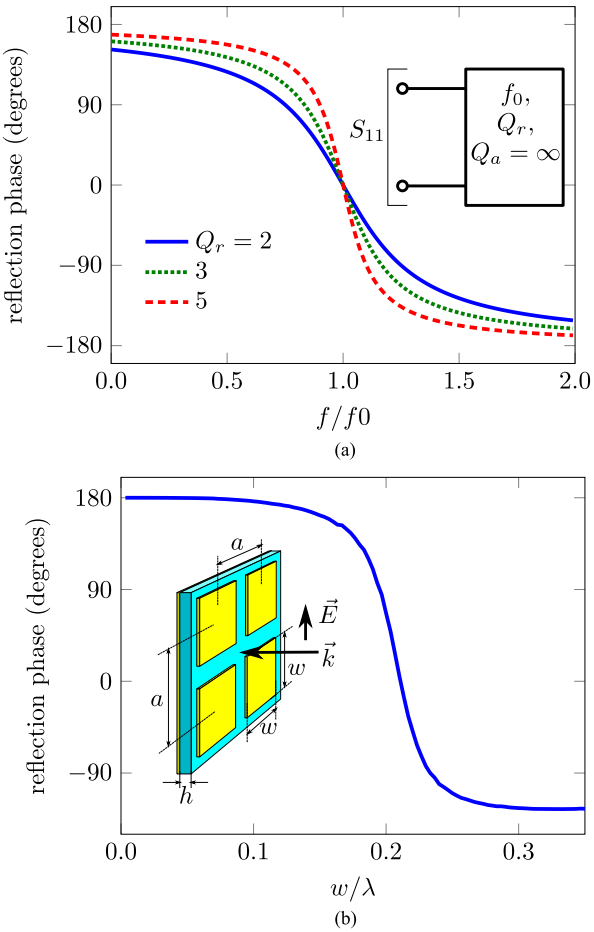

Fig. 2. Phase control using passive reflective resonators, presented (a) abstractedly, as reflection coefficient of a lossless one-port network, and (b) with the reflection coefficient of an idealized metal patch array, in which $a = \lambda/2$ and $h = \lambda/15$. The relative permittivity of the dielectric spacer is equal to 4.

In order to illustrate the technique of tuning resonance frequency by means of geometric parameters, an idealized example is contrived, and is shown in the inset of Fig. 2(b). In this example, an infinite, homogeneous array of square metallic patches is separated from a ground plane by a dielectric spacer ($\epsilon_r = 4$), and is excited with normally-incident radiation. Both the dielectric and the metal are lossless, and hence $Q_a = \infty$. This structure is investigated with full-wave simulations, and parametric analysis is performed in order to determine how response changes with respect to change in patch dimensions. Results in Fig. 2(b) show decreasing phase response with respect to increasing patch width w. This is because an increase in patch dimensions will result in an increase in the wavelength of the corresponding resonance frequency. As such, the phase characteristic shown in Fig. 2(b) corresponds closely to that which is shown in Fig. 2(a); a larger patch results in a lower value of f_0, and a higher value of f/f_0. It is also worth noting that this square patch resonator is just one example of a prospective array element [15], and that there is significant choice and freedom in the selection of the individual resonator, with benefits and tradeoffs in each case.

It can be seen from Fig. 2(a) that the gradient of the phase descent depends on the radiation quality factor Q_{r}. A larger value will result in a steeper descent, and in practical cases, can produce a larger phase tunability range. However, for a lossy resonator (i.e. $Q_{\mathrm{a}} < \infty$), this comes at the cost of increased dissipation. Additionally, a steep phase gradient is inherently more sensitive to tolerances, as a minor change to resonance frequency produces a large change in phase response. As such, there is a tradeoff associated with the quality factor. Good practice is to select the minimal value that provides the required phase tunability range.

C. Reflectarray Design

The two concerns of resonator design and phase distribution are integrated to produce a nonuniform array of reflective resonators. The phase response of each resonator in the array is determined by the desired phase distribution, e.g. with Eqs. (1) or (4), whilst accounting for the phase of the incident wave. The resonator dimensions needed to achieve this phase response are determined by parametric analysis. Each resonator thus imparts a local phase response on the reflected field, and the overall phase distribution is the aggregation of all such local responses.

There are some well-known limitations and approximations to this approach to reflectarray design, pertaining to inter-element coupling. Firstly, the design of a resonator typically operates under the assumption of an infinite array of identical elements with uniform plane-wave excitation. In practice, however, excitation is provided by nonuniform sources such as Gaussian beams. As such, the amount of energy incident upon a given element may differ from that of its neighbors, which can influence inter-element coupling effects. Secondly, the reflectarray must necessarily be nonuniform in order to achieve any useful beam-shaping operation, and this is not consistent with the unit cell assumption of total uniformity. Thus, the fact that neighboring elements are not identical breaks resonator symmetry, which can excite asymmetrical modes of resonance and significantly impact the resultant phase response [55]. The first issue can be discounted by the fact that the field distribution changes gradually, and hence a given element effectively experiences locally-uniform excitation. The second issue, however, is more challenging to address. Most often it is asserted that the change in resonator dimensions is sufficiently gradual that differences between immediate neighbors is negligible, or very close to negligible. This is often referred to as the assumption of local periodicity. However, this ceases to be accurate when steep phase gradients are required, for example, when designing flat lenses of high numerical aperture. In some such cases, parametric unit cell analysis is treated as a guideline, and individual elements are optimized in their array configuration, but this becomes extremely labor-intensive for any reasonably complicated design.

III. Fabrication of Terahertz Microantennas

Up to now, frequency has been considered abstractedly, as the fundamental principles of electromagnetics are invariant upon specific choice of frequency. However, in practical cases,

materials have frequency-dependent properties. For instance, whilst metals are good conductors in the microwave range, their conductivity decreases with increase in frequency to the point where their behavior is closer to that of lossy dielectrics in the optical range [58]. Additionally, physical device size is always relative to wavelength, and particular fabrication methodologies are better-suited to specific physical scales. Thus, specific techniques for controlling radiation are most practical for certain frequency ranges. This accounts for why, as previously discussed, early development of reflectarrays was dominated by metallic resonators separated from a ground plane by a dielectric layer, not conceptually dissimilar from that which is presented in Fig. 2(b) [10]. For the purposes of this paper, we will focus on fabrication methodologies relevant to the terahertz range.

Two broad classes of resonator are presented in this work, namely metallic and dielectric resonators, and the fabrication methodology for each is discussed in this section. All reflectarray devices that are presented in this work operate at the frequency of 1 THz, where a free-space wavelength is equal to 300 μm. Several key microfabrication techniques can therefore access the relevant physical scales. For instance, spin-coating of elastomeric polymers can be employed in order to realize a dielectric spacer in the order of a few tens of microns [59]. Vacuum-based evaporation techniques, such as electron beam deposition, can produce metal films of thickness greater than a skin-depth in the terahertz range, which is necessary for operation as a good conductor [60]. Additionally, techniques such as wet chemical etching [61], [62] and deep reactive ion etching (DRIE) [63]–[65] can define structures of sizes amenable to interaction with terahertz radiation.

The construction of the metallic resonator is given in Fig. 3(a). In order to realize this structure, first a polished silicon wafer, to be employed as structural support, is cleaned with solvents. A platinum film is then deposited onto the wafer by electron beam evaporation, using titanium as an adhesion layer. This film is thicker than a skin depth in the terahertz range, and hence the metal film operates as a ground plane, which shields the supporting wafer from radiation. A polydimethylsiloxane (PDMS, for which $\epsilon_r \sim 2.25$ and $\tan\delta \sim 0.06$ [66] at 1 THz) liquid pre-polymer is spin-coated onto the platinum ground plane, and is subsequently cured. A gold layer is then deposited onto the PDMS layer via electron beam evaporation, using chromium as an adhesion layer. Lastly, photolithography and wet chemical etching are employed to define the resonator structures. The use of platinum in the ground plane, as opposed to higher-conductivity metals such as gold, is to ensure selectivity during the wet chemical etching process. A micrograph of an example of a terahertz metallic resonator array of this sort is given in Fig. 3(b), showing highly regular planar resonators.

The second class of resonator considered in this work is the dielectric resonator. The construction of the dielectric resonator is given in Fig. 3(c), and the fabrication procedure employed to realize these resonators is as follows. A gold ground plane is deposited on a silicon supporting wafer with electron beam evaporation, using chromium as an adhesion layer. Subsequently, the dielectric that comprises the resonator structure is bonded to the ground plane. The efficient operation of such resonators is dependent on a low-loss dielectric with moderate-to-high relative permittivity for this purpose, and high-resistivity float-zone intrinsic silicon (HR Si, for which $\epsilon_r = 11.68$ and $\tan\delta < 4 \times 10^{-5}$ [67] over a broad bandwidth) is selected as suitable. However, a significant challenge to the realization of such resonator structures is the integration of relatively thick single-crystal silicon on a metallic substrate. This is addressed by spin-coating a 0.5 μm-thick adhesion layer of SU-8 onto the gold-coated wafer, prior to bonding a HR Si wafer to the SU-8. Bonding is performed by passing the structure through a table-top laminator, which cures the SU-8, resulting in a strong bond between the metal film and HR Si wafer. Subsequently, the HR Si wafer is thinned to the required thickness using a DRIE process. Photolithography is then employed in order to define the patterns corresponding to required resonator shape, and a second DRIE process is employed to etch away the dielectric material surrounding the resonator structures. A micrograph of an example of a terahertz dielectric resonator array of this kind is given in Fig. 3(d), showing high-quality cylindrical structures with well-defined edges, which validates the fabrication procedure.

IV. Metallic Resonator Reflectarrays

This section summarizes the design and experimental characterization of three different metallic resonator-based terahertz reflectarrays. All devices presented in this section are far-field deflectors of the type illustrated in Fig. 1(a,b,e). As such, their intended beam-shaping operation is to steer incident radiation away from the specular reflection path. As explained in Section II-A, a deflector requires a sawtooth phase distribution, with each period covering a 360° cycle. Owing to the periodicity of this phase distribution, the deflection angle θ_s can be determined in accordance with the diffraction grating equation,

$$\sin\theta_s = \frac{s\lambda}{D} - \sin\theta_i, \quad s = 0, \pm1, \pm2, ..., \tag{7}$$

in which λ is the free-space wavelength, θ_i is the angle of incidence, D is the grating period, and s is the diffraction order. For a deflector, the steering operation generally corresponds to first-order diffraction (i.e. $s = \pm1$). When implemented with an array of discrete resonators, this translates to a progressive phase shift of $\Delta\varphi$ between adjacent elements, which is related to the deflection angle by the following expression, for all diffraction orders,

$$\sin\theta_s = \frac{s\Delta\varphi}{ak_0}. \tag{8}$$

In all deflector designs in the present work, a full phase cycle fits into a discrete number of elements, m, and hence the grating period can be expressed as $D = ma$, and the progressive phase shift is simply,

$$\Delta\varphi = \frac{360^\circ}{m}. \tag{9}$$

Thus, the design of the total array is adequately described by a single period of the array, which is henceforth referred to as the "sub-array", or the less well-known "super-cell". The required

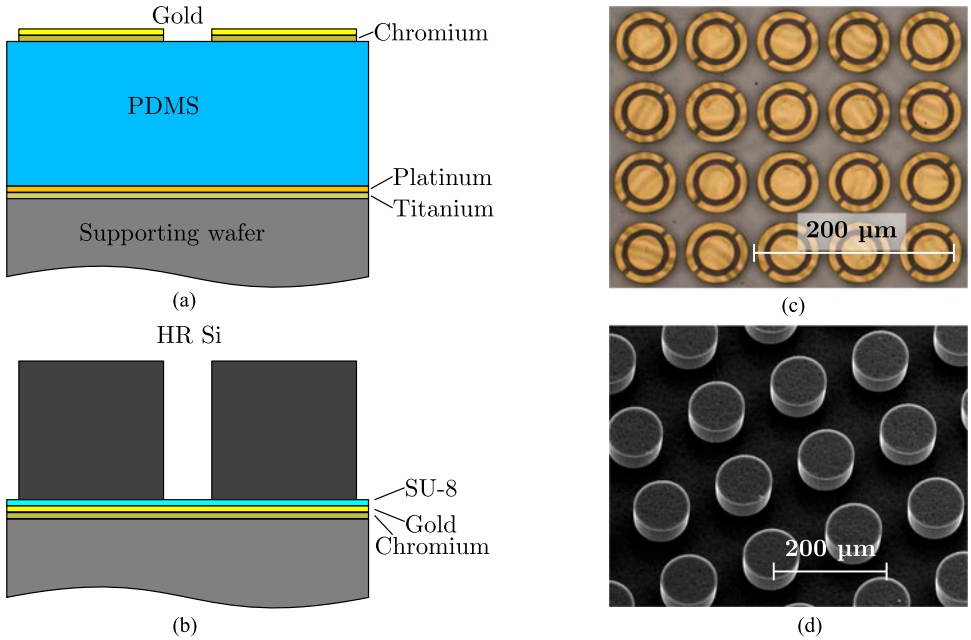

Fig. 3. Structure of resonators of the sort presented in this work, showing (a) gold metallic resonators separated from a platinum ground plane by a polymer dielectric, (b) micrographs of terahertz resonators of metallic resonators of this sort, reproduced with permission from [56], (c) dielectric resonators affixed to a gold ground plane by means of an adhesion layer, and (d) micrographs of dielectric resonators of this sort, reproduced with permission from [57].

phase response of each resonator can be straightforwardly expressed in discrete fashion,

$$\varphi_n = 360^\circ \frac{n}{m} + \varphi_0, \quad n = 0, 1, 2, ..., m-1, \qquad (10)$$

where φ_0 is some arbitrary baseline phase. It is worth noting that the total phase range to be covered by the resonators is not 360° exactly, but rather $\frac{m-1}{m}360^\circ$, as a value of 360° is equivalent to 0°. As such, a smaller phase range is required for a coarser phase quantization, which is useful in instances in which the total 360° range is not practically achievable.

Note that (7) is only valid for $D > \lambda$, i.e. non-subwavelength grating period, in contrast to the requirements of the individual resonator discussed in Section II-B. Thus, for deflecting reflectarrays of this sort, if the lattice constant is fixed then the deflection angle is determined by the choice of sub-array size, m. As such, this approach does not provide much freedom for the selection of the output deflection angles. For instance, if a lattice constant of $a = \lambda/2$ is employed under normal incidence, the possible values of θ_s are 41.8°, 30.0°, 23.6°, 19.5°, and so on, which may be too coarse for some applications. However, other angles are available if the sub-array contains multiple 360° phase cycles, where a single cycle does not fit into an integer number of elements. In this way, there is more freedom in the selection of phase gradient. However, the single-cycle sub-array approach is selected in this instance for simplicity, as it is sufficient for a proof-of-concept.

As explained in Section II-C, the coupling between nonuniform elements can lead to inconsistencies between the reflectarray operation and unit cell design. To mitigate this, resonator dimensions are adjusted in order to optimize the reflectarray for maximal power deflected into the desired direction. The sub-array design approach makes this possible, as there is a manageable number of elements requiring adjustment.

A. *Isotropic Deflection Reflectarray*

This device employs a square patch as the resonator unit cell [40]. As discussed in Section II-B, a larger patch will result in a lower resonance frequency, and hence a greater negative phase shift. Thus, the patch size is designed to monotonically increase across the sub-array. A diagram of the sub-array, illustrating the intended beam shaping operation, is shown in Fig. 4(a). Terahertz radiation is incident at an oblique angle, and is deflected away from the specular reflection path, towards the surface-normal. There are six elements in the sub-array for this design, and hence the required progressive phase between neighboring elements is 60°. The lattice constant is 140 μm, the operating frequency is 1 THz ($\lambda = 300$ μm), and the incidence angle is 45°, and hence the grating equation gives an output angle of -20.5°.

Full-wave simulations are employed to investigate the reflection response of the unit cell. As in Section II-B, this is modeled as a uniform array of infinite extent that is excited by a normally-incident plane wave. The fourfold symmetry of the patch results in isotropic response, and hence no particular polarization vector need be specified. Parametric analysis based on these full-wave simulations is employed in order to determine the required patch dimensions to produce progressive phase between adjacent elements, and to this end, the patch side-length is swept in increments of 1 μm. Results are shown in Fig. 4(b). It can also be seen from these results that the maximum loss is in the order of 1.2 dB, which is acceptable for such a frequency range.

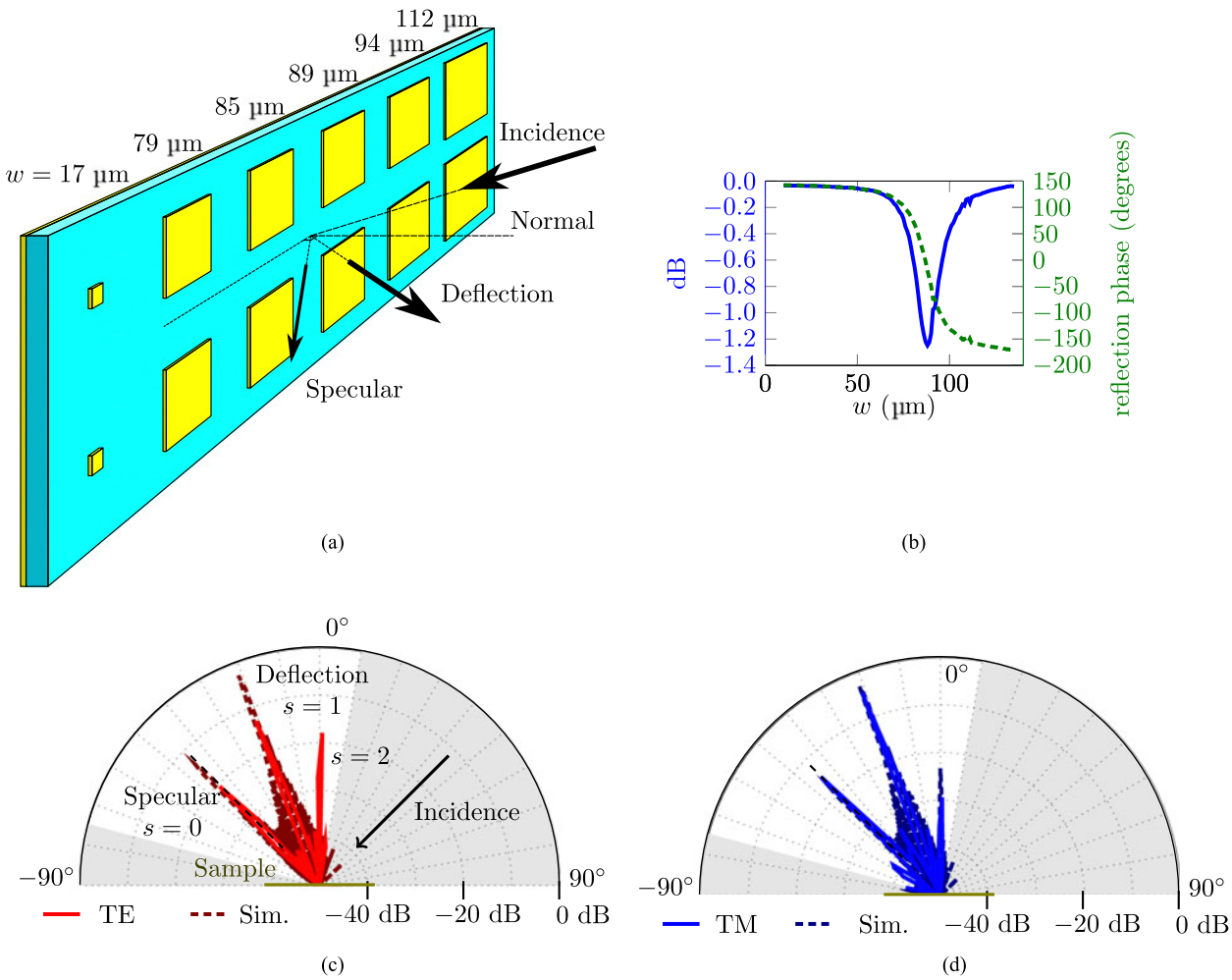

Fig. 4. Isotropic metallic resonator reflectarray, showing (a) two sub-array periods with intended operation, where lattice constant $a = 140$ μm and dielectric thickness is $h = 15$ μm, (b) parametric analysis of side-length of square patch at 1 THz, and (c) and (d) radiation patterns of fabricated reflectarray at 1 THz, for TE and TM polarizations respectively, with diffraction order indicated for each major peak, and angles not covered by the scan are greyed-out. Simulated radiation patterns are also given for comparison, where it is noted that the sidelobe level is higher than in measured results due to uniform, non-Gaussian excitation.

This design is fabricated in accordance with the procedure described in Section III, and its radiation pattern is experimentally characterized with a goniometric terahertz time-domain spectroscopy (THz-TDS) setup. In this experiment, the sample is excited with obliquely-incident radiation at a 45° angle, by an emitter that is held in a fixed position. A detector is scanned in a sample-centered arc, from $-75°$ to 10°, taking THz-TDS measurements at 2° intervals, and a gold mirror is used as a reference. This procedure is performed for both TE and TM polarizations, and the resulting radiation patterns are shown in Fig. 4(c). It can be seen for both polarizations that the radiation maximum is as intended at $\sim -21°$, rather than the specular direction of $-45°$. A good overall judge of the performance of such a device is the sidelobe level, as this is telling of the fidelity with which the intended phase distribution has been produced by the reflectarray. For this device, the sidelobe level of the TM polarization is $\sim$10 dB lower than the main lobe, whereas for TE it is $\sim$5 dB, and hence the TM-performance is superior. This disparity is partly due to the oblique incidence, as the different polarizations see distinct effective projected patch sizes. It is deduced that the TM-polarized wave is less strongly affected by the oblique incidence than TE. It is also worth noting that the use of THz-TDS in the measurement makes it possible to evaluate that the -3 dB spectral bandwidth of the measured peak is $\sim$5%. This limited bandwidth is evidence of the previously-noted dispersion exhibited by flat beam control devices of this sort.

B. *Polarizing Beam Splitter*

If rectangular patch resonators are employed, rather than square, then the resonator will exhibit birefringent response. This is because the wavelength that produces a standing wave along the long-edge dimension will be lower in frequency than for the short-edge dimension. As such, it is possible to engineer rectangular patches that interact very strongly with one polarization, causing significant phase shift, but leave the orthogonal polarization unaltered, for a given operating frequency. For this design, this birefringent rectangular patch concept is employed in order to realize a deflector reflectarray that manipulates the TE and TM polarizations of normally-incident radiation separately [41]. Engineerable birefringence of this sort is a highly

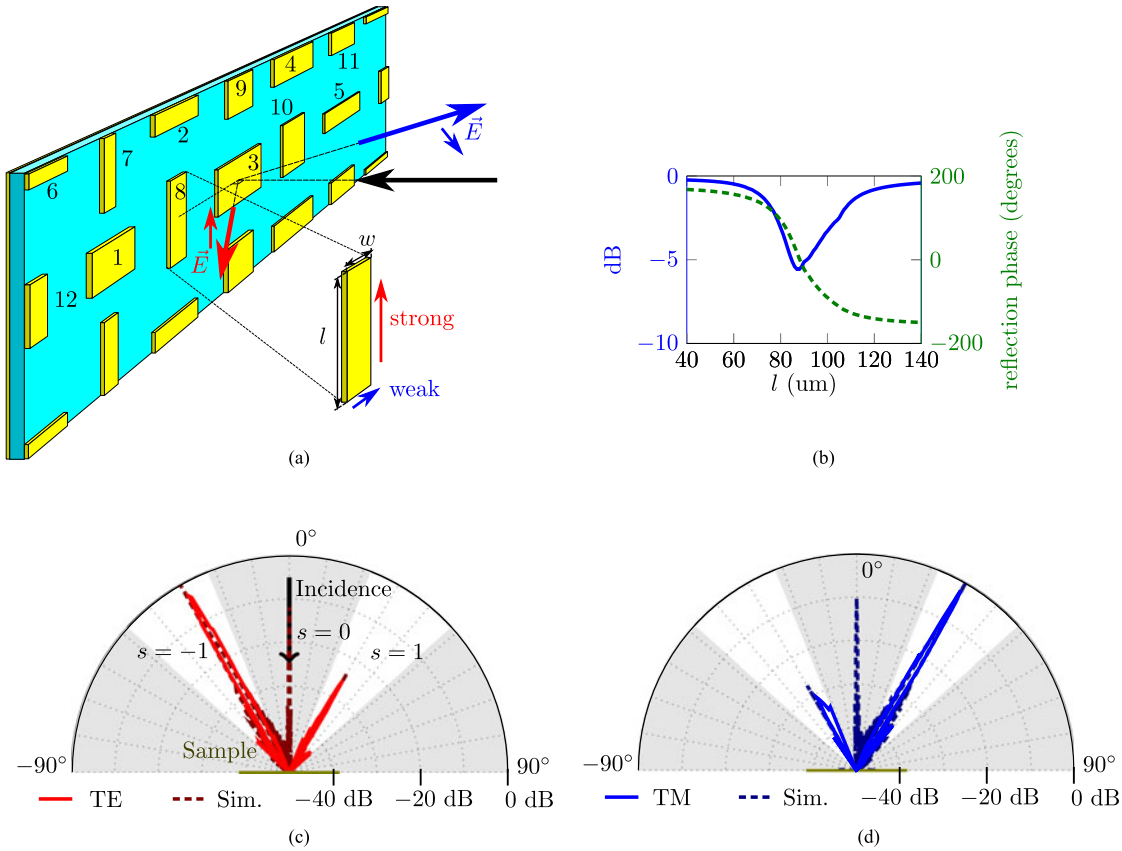

Fig. 5. Polarizing metallic reflectarray, showing (a) sub-array design, with illustration of intended operation, where all patches are numbered to show correspondence with the dimensions given in Table I, lattice constant $a = 100$ μm, and dielectric spacer thickness $h = 20$ μm, (b) parametric analysis of rectangular patch length at 1 THz, for polarization parallel to long-edge, and (c) and (d) radiation patterns of fabricated reflectarray at 1 THz, for TE and TM polarizations respectively, with simulated results for comparison. Angles not covered by the scan in the measurement are greyed-out.

desirable property for reflectarray antennas in communications applications. This is because orthogonal polarizations can be manipulated independently, which can be used to provide two orthogonal channels in the same link.

It is possible to use a single rectangular or cross-shaped patch to interact with both polarizations, but this can result in the excitation of an undesirable cross-polarization component due to symmetry-breaking in the inhomogeneous array. As such, we opt for an alternative arrangement, as shown in Fig. 5(a). The unit cell effectively contains two different rectangular patches; a horizontally-aligned patch to interact with the TM polarization, and a vertically-aligned patch to interact with TE. In order to allow for clearances and mitigate strong coupling, whilst maintaining the sub-wavelength periodicity, these differently-oriented patches are staggered. As with the previous design, a progressive phase difference is achieved by varying patch dimensions. By monotonically increasing the length of the TE-patches in one direction, whilst decreasing the length of the TM-patches in the other, the TM polarization is deflected to a positive angle, whilst the TE polarization is deflected to a negative angle. As the sub-array size is common to both polarizations, the deflection angle is symmetrical for this design. In this instance, the grating period is $D = 600$ μm, resulting in a deflection angle of $\pm 30^\circ$ for the normal incidence employed. Asymmetrical deflection angles are also possible, but this requires a different array period for each polarization. In order to incorporate both, the width of the sub-array must be the least common multiple of the two individual periods [68].

In order to minimize loss over the relevant phase tunability range, and provide a gradual phase characteristic, patch width is varied with patch length in accordance with the following piecewise-linear expression, for which all units are micrometers,

$$w = \begin{cases} 32 + 0.2l, & \text{if } l \in [40, 90], \\ 230 - 2l, & \text{if } l \in [90, 105], \\ 20, & \text{if } l \in [105, 140]. \end{cases} \tag{11}$$

By making patch width dependent on patch length in this way, we reduce the number of independent variables to one. Additionally, for a given patch, the impact of the nearest orthogonally-polarized neighbor is small, and can therefore be neglected. Lastly, due to the normal incidence, orthogonal polarizations can be considered equivalent for patches rotated through 90°, and hence a single parametric sweep can describe both polarizations adequately. These factors simplify parametric analysis significantly by reducing the search-space. Parametric analysis of patch length is performed using full-wave simulations, and the results are shown in Fig. 5(b). For this analysis, the polarization of incident radiation is parallel to the long edge of the

TABLE I
OPTIMIZED BIREFRINGENT PATCH DIMENSIONS

Element	long-edge dimension, l (μm)	short-edge dimension, w (μm)
1	55	38
2	75	48
3	85	49
4	91	50
5	100	30
6	122	24
7	120	20
8	97	34
9	88	45
10	82	52
11	76	48
12	55	43

rectangular patch. As before, a unit cell approach is employed, and side length is swept in increments of 1 μm. The results show a large phase tunability range, but it is also worth noting that the loss is greater than in the previous design. This increased loss is intrinsically linked to the narrow patch geometry, and hence there is an evident tradeoff between engineered birefringence and efficiency. In the final design, mutual coupling effects that are not accounted for in the unit cell analysis were mitigated by fine-tuning the dimensions of the individual patches. The final configuration of the sub-array is given in Table I, with element number corresponding to the diagram in Fig. 5(a).

As before, this device is fabricated, and characterized with THz-TDS, using a goniometric setup to measure the radiation pattern. In this instance, excitation is in the surface-normal direction, and wire-grid polarizers are employed in order to isolate and test the TE and TM polarizations individually. Due to practical constraints of laboratory clearances, the scanning range is limited to the ranges -48° to -22°, and 22° to 48°. The results of this procedure are shown in Fig. 5(c), and it can be seen from the radiation patterns that the TE polarization is indeed deflected to -30°, and the TM polarization is deflected to $+30^\circ$. Due to feed blockage, it is not possible to characterize the amount of energy lost to specular reflection directly, but full-wave simulations given in the same plot indicate that the difference between deflected and specular reflection is greater than 10 dB. If it is desirable to experimentally characterize the specular reflection directly, a pellicle beam splitter can be deployed for this purpose. However, this approach is not used in the present work due to practical constraints.

C. Polarizer-Based Reflectarray

A wire-grid polarizer is a device consisting of regularly-spaced, parallel striplines. The separation and width of the striplines are both deeply sub-wavelength, but the striplines themselves are far longer than a wavelength. As a consequence of this, the interaction of incident electromagnetic radiation with the wire-grid polarizer will depend on the polarization. The polarization that is parallel to the orientation of the striplines is able to induce a current in the striplines, and as the striplines are extremely long, no standing wave pattern is established. As such, the incident wave effectively sees a short circuit, and is therefore reflected. However, for the orthogonal polarization, the conducting portions are interrupted by gaps, and as the spacing is deeply subwavelength, the currents induced in this dimension are negligible. As such, this polarization is not strongly affected by the striplines, and it is transmitted. Therefore, a wire-grid polarizer is ideally a device that simply reflects one polarization, and passes the orthogonal polarization.

For the third and final metallic resonator-based device presented in this work, the concept of a wire-grid polarizer is incorporated into a reflectarray design [42]. This is achieved by using deeply-subwavelength metallic striplines to make up both the ground plane and the resonant patches in the reflectarray. The result is a reflectarray that deflects one polarization, and passes another, as shown in Fig. 6(a). For the resonator element, stripline segments are arranged so as to collectively approximate a square patch that interacts with the TE-polarization exclusively. The stripline width is 5 μm, and the separation between striplines is 5 μm. As such, although the resonator is intended to approximate a square patch, the horizontal width of this patch is necessarily rounded-down. For this design, the grating period is $D = 560$ μm, resulting in a deflection angle of $\sim 32^\circ$ under normal incidence.

As before, parametric analysis is employed in order to determine the required patch sizes for the array, and the results are presented in Fig. 6(b). For the TM-polarization, the majority of the power is simply passed, and the size of the resonator exhibits negligible impact upon the transmitted power, as intended. It can also be seen that the TE polarization exhibits a reasonably large phase tunability range on reflection, albeit with loss comparable to the previously presented design.

In order to observe the TM-polarized transmission, the use of a supporting silicon wafer must be abandoned for this design. As such, the procedure described in Section III is modified. A 100 μm-thick layer of PDMS is spin-coated directly onto the supporting wafer, and the stripline ground plane is patterned onto this layer. Thereafter, the procedure continues as previously described, and the PDMS structure is lifted-off from the supporting wafer after the resonators are etched. The 100 μm-thick PDMS layer acts as a support for the structure after lift-off. The radiation pattern of the fabricated structure is experimentally characterized with a goniometric setup, which scans with a angular resolution of 0.5° over a range from -155° to $+155^\circ$ (in the positive-angle direction). Both polarizations are tested in this way, and the results are presented in Fig. 6(c). It can be seen that the TM-polarization is passed, and the TE-polarization is deflected to a 32° angle, as expected. Additional to that, full-wave simulations given in the same plot indicate that specular reflection is $\sim$12 dB lower than the deflected peak. Lastly, the absence of a supporting wafer makes the sample intrinsically elastic, as is typical of elastomers such as PDMS As such, it is possible to stretch the sample by $\sim 10\%$, which increases the sub-array size, and hence reduces the deflection angle by a few degrees.

V. DIELECTRIC RESONATOR

One of the most pressing issues that arises from the use of terahertz metallic resonators in the previous section is low efficiency.

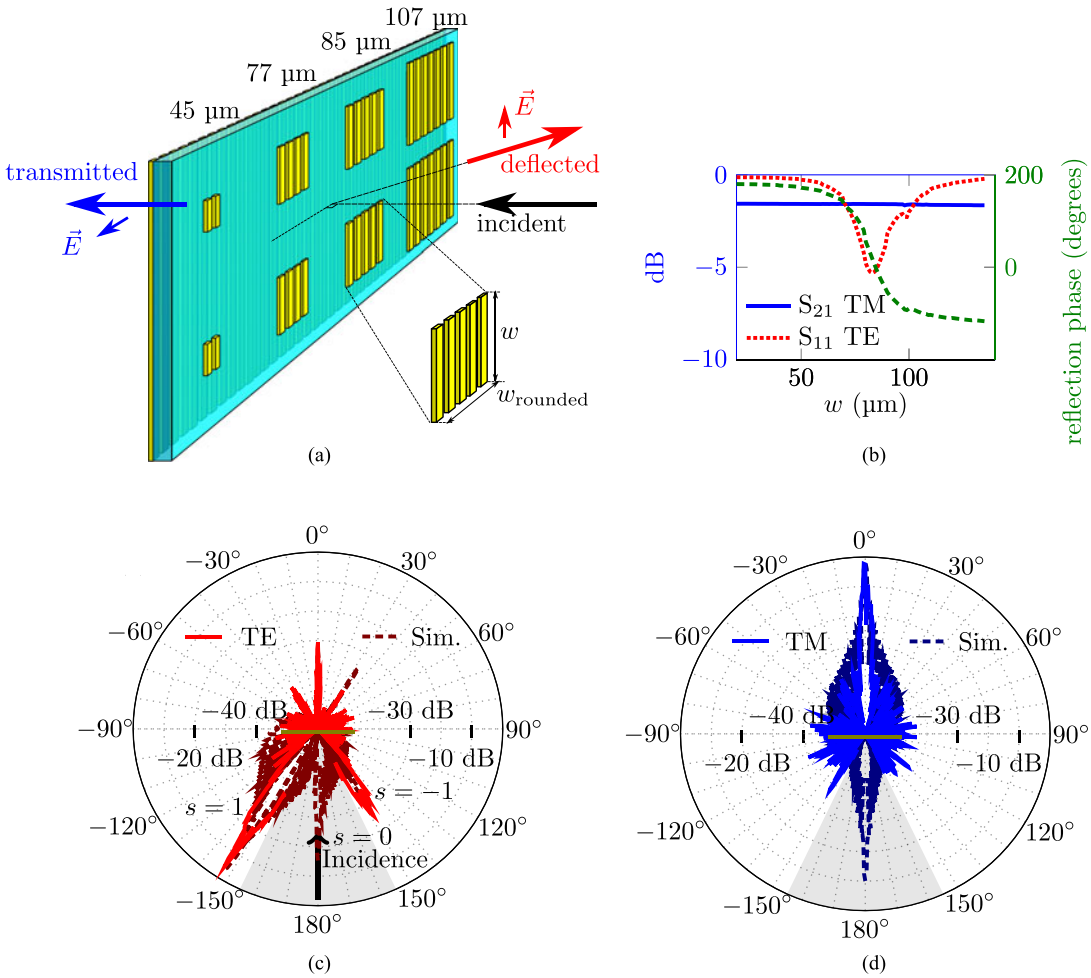

Fig. 6. Stripline polarizer-based reflectarray, showing (a) two sub-array periods, illustrating intended operation, where lattice constant $a = 140$ μm and dielectric thickness $h = 20$ μm, (b) parametric analysis of resonator unit cell at 1 THz, and (c) and (d) radiation patterns of fabricated reflectarray at 1 THz, for TE and TM polarizations respectively, with simulated results for comparison. Angles not covered by the scan are greyed-out.

This is most apparent in the latter two examples given, where parametric analysis shows peak reflection loss up to ∼5 dB, which corresponds to ∼70% of incident power being dissipated. Although this level of loss only applies to specific resonators rather than the total array, it is still cause for concern. The dissipation loss in these metallic resonators is mainly due to the choice of PDMS ($\tan\delta = 0.06$) as the dielectric spacer. This material is moderately lossy, and this loss is exacerbated dramatically by field confinement due to resonance of conduction current. Terahertz resonators using a lower-loss polymer dielectric for the spacer have previously been demonstrated [69], but the loss in such materials can rarely be considered negligible. Furthermore, although metals are reasonable conductors at terahertz frequencies, they are far from ideal conductors. As such, the fact that metallic resonators make use of conduction current in their mode of resonance makes them susceptible to Ohmic loss. Thus, the efficiency of metallic resonators in the terahertz range is intrinsically limited, and this fact pinions us to investigate alternative means of devising a reflective resonator for operation in the terahertz range.

A popular alternative to the metallic resonator is the dielectric resonator, and a brief summary of its resonance mechanism is as follows. A strong discontinuity in refractive index at a dielectric boundary will result in significant reflection of electromagnetic energy. For example, a wave originating in a dielectric of moderate-to-high refractive index (i.e. $n > 3$), upon encountering a boundary to free space, will reflect the majority of its energy back into the dielectric. Thus, a small volume of this dielectric will behave as a resonant cavity, since a wave will reflect internally off one boundary, only to reflect off another, forming a standing wave at certain particular resonance frequencies. A given dielectric resonator may have numerous such non-harmonic modes of resonance that conjoin to deliver an overall phase range much larger than 360°. The characteristics (i.e. f_0, Q_{r}, and Q_{a}) of each mode of resonance will be dependent on the resonator's structure and dielectric properties. As the resonance of a dielectric resonator is of displacement current, as opposed to conduction current, its Ohmic dissipation is considerably lower than for metallic resonators.

If such a resonator is intended to couple to free-space fields, it can be considered a dielectric resonator antenna (DRA). Typically this is achieved by leaving the resonator unshielded, and constructing it out of sufficiently moderate-index dielectric material. Antennas of this form were initially conceived of as an

efficient alternative to metallic resonators at millimeter-wave frequencies and beyond, where metals cease to behave as near-ideal conductors [70]. The dielectric that is employed in the present work is HR Si, and a description of how DRAs are constructed from this material is given in Section III. It is worth noting that these DRAs are situated on a gold ground plane, which makes some contribution to Ohmic loss. However, this is less of a concern than in the case of the metallic resonator, as the standing wave pattern on-resonance is confined to the dielectric, and not the metal [71].

A. *Artificial Magnetic Conductor*

Since prior work on DRAs at terahertz frequencies is limited, it is desirable to know the unit cell behavior of the HR Si DRA in more detail than previous metallic resonator examples. As such, experimental means are employed to characterize the unit cell, and in doing so, validate the associated fabrication procedure. To this end, a homogeneous array of cylindrical DRAs is fabricated, with lattice constant $a = 150\ \mu$m, radius $r = 50\ \mu$m, and height $h = 50\ \mu$m [57]. This configuration is illustrated in Fig. 7(a). The response to TE-polarized, obliquely-incident radiation impinging at a 45° angle is characterized using THz-TDS, where it is noted that an iris is employed to limit the lateral extent of the beam to the patterned portion of the sample, and results are given in Fig. 7(b,c). This result is compared to both full-wave simulations and to modal analysis of the form described in Section II-B, which makes use of (6), and strong agreement is attained for phase response in Fig. 7(c). The measured magnitude response in Fig. 7(b), however, is not strictly consistent with the modeled results, most notably when the magnitude response appears to exceed unity. It is asserted that, given that magnitude is less reliable than phase in THz-TDS [72], [73], it is likely that the quality of the experimental results is sufficient to confirm the phase response, but not the magnitude response. This is potentially related to reduction in dynamic range due to the iris, which produces some variation in the measured results. As the mean position of the curve is so close to 0 dB, this variation translates to the aforementioned greater-than-unity response observed. Additionally, it is possible that there are array coupling effects pertaining to the disparity between the finite size of the excitation beam and the infinite size of the modeled array. Essentially, a given DRA can couple additional energy into a neighbouring element that is comparatively weakly-excited. This alters the effective aperture of the reflected beam, and causes an increase in magnitude that is not observed in simulation.

At ∼0.78 THz, the magnitude response of the uniform array is very close to unity, and the phase response is ∼0°. This means that the electric field vector of the reflected wave is in-phase with that of the incident wave, and of roughly the same magnitude. This is in contrast with the phenomenon of reflection from a PEC surface, in which the electric field vector is inverted. Reflection of an electromagnetic wave is always accompanied by reversal of one of either the electric or magnetic field vectors, as the propagation vector is determined by the cross-product of these two vectors. Since the electric field vector is not inverted for this uniform DRA array, but reflection is observed, this means that the magnetic field vector must be inverted. As such, this device can be considered an artificial magnetic conductor, for frequencies in the neighborhood of 0.78 THz. Such artificial magnetic conductor devices are useful for applications in the development of compact antennas [74]–[76], and hence the demonstrated device has potential for terahertz antenna technology.

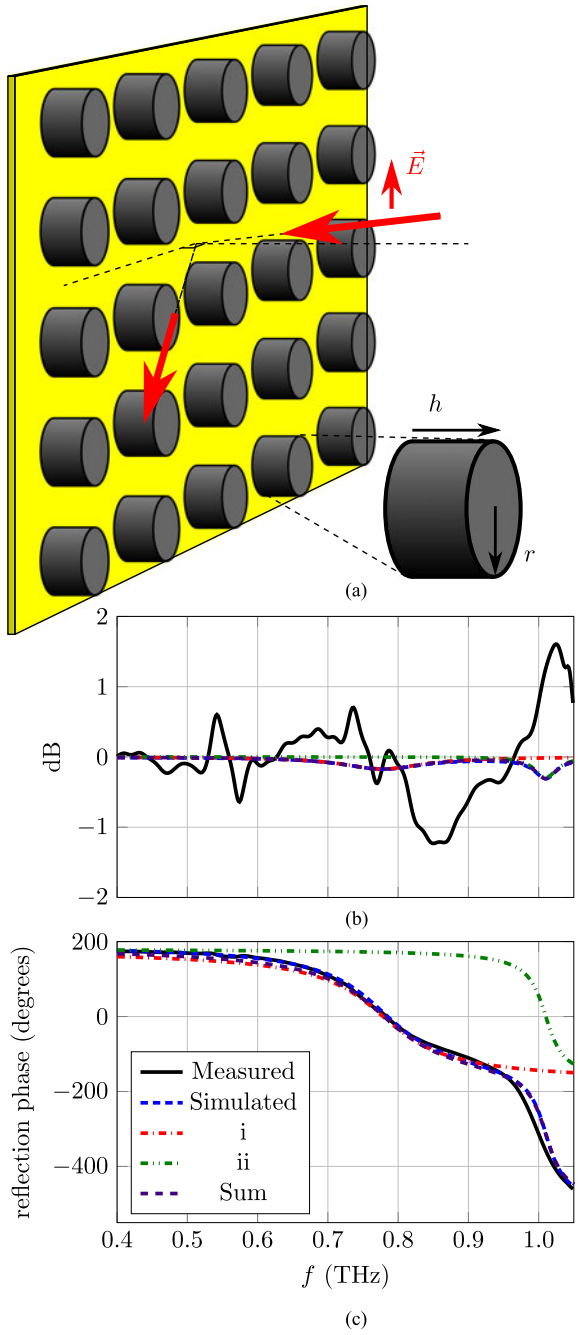

Fig. 7. Homogeneous array of cylindrical DRAs, showing (a) array structure, with oblique incidence and specular reflection of TE-polarized radiation shown, and (b,c) magnitude and phase response of homogeneous DRA array under such excitation, using experimental characterization, full-wave simulation, and analytical techniques described in Section II-B. Curves (i) and (ii) both describe single modes of resonance, with $f_{0,i} = 0.778$ THz, $Q_{r,\mathrm{i}} = 5.5$, $Q_{a,\mathrm{i}} = 560$, $f_{0,\mathrm{ii}} = 1.01$ THz, $Q_{r,\mathrm{ii}} = 26$, and $Q_{a,\mathrm{ii}} = 1534$.

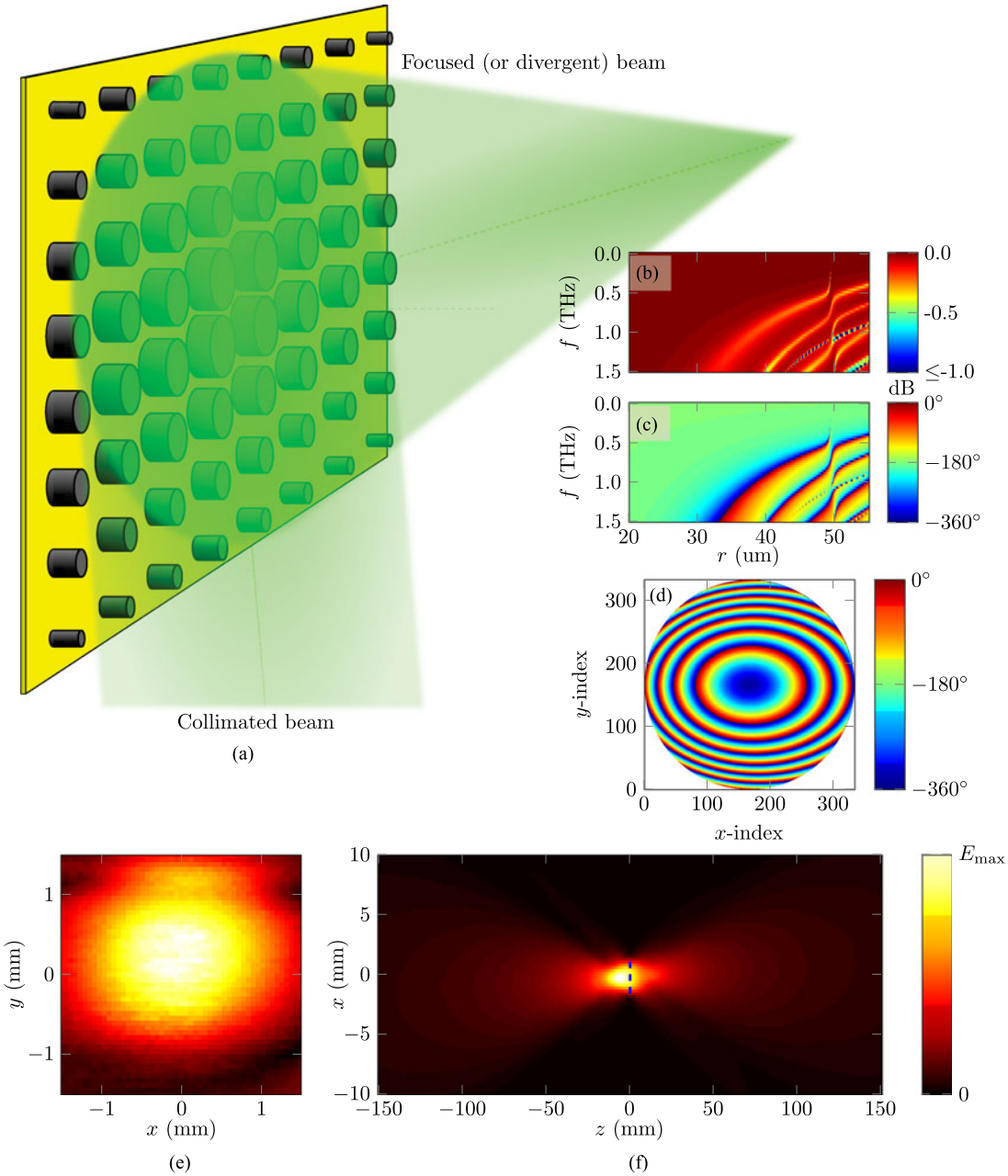

Fig. 8. DRA-based focusing reflectarray, showing (a) diagram of operation and structure (not to scale), (b) and (c) broadband parametric analysis of DRA unit cell radius, (d) required phase response for oblique lensing at a 45° angle and a focal length of 150 mm, (e) measured focal spot at 1 THz, when excited with a collimated beam, and (f) approximate path of focused beam, as extrapolated from the focal spot using scalar diffraction theory.

B. Lensing Mirror Reflectarray

The beam-shaping operation that is selected as proof-of-concept for the DRA-based reflectarray is lensing. Essentially, this means the designed device can transform a collimated beam into a focused beam of a given focal length, and hence by the principle of beam reciprocity, it can also transform a divergent beam of the appropriate curvature into a collimated beam. This is equivalent to the operation illustrated in Fig. 1(c,f), however in this instance, radiation is obliquely-incident at 45°, which is necessary to mitigate feed blockage for experimental characterization. This beam-shaping operation is illustrated in Fig. 8(a). Note that a design of this sort cannot straightforwardly be decomposed into sub-array periods, as with the previously given deflecting reflectarray examples, and hence the entire array design must be considered at once.

Cylinder radius is identified as the appropriate geometric parameter for phase control, as the fabrication procedure given in Section III requires that all HR Si features have the same height. As such, parametric analysis using full-wave simulations is performed on cylinder radius, and the amplitude and phase responses are given in Figs. 8(b,c) respectively. In order to illustrate the potential for resonators of this sort to cover the terahertz range, this is presented as broadband plots. It is worth

noting that, for isolated narrowband modes in this analysis, the response drops as low as -22 dB. However, such modes are not representative, and are easily avoided in array design. For this reason, the range is clipped to ≥ -1 dB in Fig. 8(b). The present reflectarray design is intended to operate at 1 THz, and with the HR Si DRA, it is possible to achieve a full 360° phase tunability range with loss no greater than 0.32 dB at this frequency. This clearly illustrates the high efficiency of DRAs of this sort.

In order to perform the lensing operation, a phase distribution similar to that which is given in (4) is required, but it must be adjusted to accommodate for the oblique incidence. This is achieved by skewing the circular characteristic into a shape that is closer to an ellipse, which is described by the following expressions,

$$d_F(x,y) = \sqrt{(x_F - x)^2 + (y_F - y)^2 + z_F^2}, \quad (12)$$

$$\varphi(x,y) = k_0 \left(d_F(x,y) - x \sin 45^\circ\right) + \varphi_0, \quad (13)$$

where (x_F, y_F, z_F) is the position of the focal point. In this instance, the focal length of the reflectarray is $F = 150$ mm, at a 45° angle with the z-axis, and hence $(x_F, y_F, z_F) = (-106.066, 0, 106.066)$. This results in the phase distribution shown in Fig. 8(d). This phase distribution is mapped to the appropriate cylinder radii, using the results at 1 THz in Fig. 8(c), and the resultant array design is fabricated. The circular layout is 333 elements in diameter, which results in a total of over 87,000 elements across the total area of the array. Note that, in the final design, cylinder radius is adjusted to account for disparities in angle of incidence introduced by the divergent beam that is incident when the device is acting as a collimator.

The fabricated reflectarray is excited with a collimated beam, and the field distribution in the focal plane is imaged using THz-TDS. The results are presented in Fig. 8(e), showing a clearly-defined focal spot, albeit with some minor aberration. Note that the Cartesian axes defined in these results are separate to those described in (12) and (13). It is desirable to know the field distribution of the propagating focused beam in more detail, and to this end, scalar diffraction theory is employed [50]. The focal spot is back-propagated through a single focal length, and then forwards-propagated through two focal lengths, in order to reconstruct the beam. The results of this procedure are shown in Fig. 8(f), for the xz-plane. Note, this procedure does not include portions of the focal plane that are outside the bounds of the measured raster scan, and therefore can only be considered an approximation. The measured and reconstructed focused beam results jointly verify that the reflectarray is capable of focusing a collimated beam, and hence that it functions as intended.

By reciprocity, a device capable of focusing a collimated beam is also capable of collimating a divergent beam. As such, this reflectarray can be used to increase antenna gain, by reducing the divergence of a given source. Analytical means have been employed to determine the antenna gain produced by this reflectarray design [10]. For this procedure, quasi-uniform illumination is assumed, and antenna gain of 48.5 dBi is determined under these conditions. This clearly illustrates the potential for DRA-based reflectarrays of this sort to realize high-gain antennas.

VI. Challenges and Outlook

In order to expedite progress towards practical applications, the field of terahertz reflectarray antennas will benefit significantly if research efforts are concentrated in certain areas. These include solid-state electronic steerability (potentially using new and novel materials), high-efficiency birefringence, reduction of dispersion, and accurate modeling of non-uniform arrays of resonators.

Firstly, all of the designs discussed in the present work are examples of static reflectarrays, i.e. their phase distributions cannot be actively reconfigured. However, such a capability is key to achieving dynamic steerability, which will likely be required for practical terahertz technologies in the future. Whilst there has been some work on dynamically-reconfigurable reflector devices for terahertz beam control based on mechanical actuation [77], solid-state, electronically-controlled devices are preferable due to superior modulation speed, versatility, compactness, and control. Granted, small arrays of coupled terahertz radiators in CMOS have demonstrated steerability at 280 GHz [78], but such devices are unlikely to scale up well in size and frequency. Thus, an electronically-reconfigurable terahertz reflectarray remains a highly sought-after achievement. As with the static reflectarray devices presented here, efficiency is key. Whilst DRAs offer high efficiency, they are unlikely to be amenable to actively-tunable control. That said, further investigation into incorporating semiconductors of variable carrier concentration [79], [80] may yield new techniques to realize tunable terahertz DRAs. In general, however, metallic resonators are more suitable for dynamic tunability, but the polymer-based resonators presented in this work will not likely be compatible with the integration of nonlinear materials for tunable devices. Therefore, we must investigate new methods for fabricating resonators that can accommodate dynamic, tunable, electronic control, whilst hopefully maintaining efficiency on-par with the DRAs presented in this work. This would facilitate dynamic steerability of terahertz radiation, which would in-turn unlock significant potential for new applications. Graphene-based resonators have previously been nominated as being potentially suitable for this purpose [37], [81], [82], owing to this material's capacity for tunability with voltage bias. Although practical demonstrations of terahertz reflectarrays of this sort are lacking, there are noteworthy efforts in this direction. Furthermore, other graphene-based devices have been demonstrated [83], which illustrates the practical feasibility of graphene-based terahertz devices. Additional to that, superconducting materials have previously been employed for tunable terahertz metamaterials [84], and this represents another potential avenue for investigation. However, the success of this approach in attracting practical applications will be dependent upon advances in high-temperature superconductors.

As discussed in Section IV, engineerable birefringence is a highly desirable property for terahertz reflectarrays. However, this comes at the cost of reduced efficiency for the terahertz metallic resonators presented in this work. This is because microstrip dipoles and thin striplines exhibit higher bulk resistance than square patches, which translates to increased losses due to Ohmic dissipation. This concern is a general one; the added demands of independently phasing two separate polarizations

will invariably impact the resonator efficiency. For a higher-efficiency birefringent resonator, one might attempt to adapt the DRAs introduced in Section V, and break their radial symmetry in order to produce a birefringent response. However, such asymmetric DRAs are highly vulnerable to detrimental effects due to coupling between heterogeneous elements. As such, engineered birefringence is challenging to realize in a DRA-based terahertz reflectarray.

Birefringence is advantageous because it can provide orthogonal channels, which effectively doubles the overall data rate in practical communications applications. Another approach to improving data rate is to increase the spectral bandwidth of a single channel by reducing dispersion. Flat beam-shaping devices of the sort presented in this work are inherently dispersive, for reasons including the phase-wrapping outside the bounds of a full cycle. However, there are efforts in the microwave range to address the issue of dispersion in reflectarray antennas by the use of a technique known as true-time delay phase compensation [85]. For this approach, phase is not wrapped in a 2π cycle, and the phase response is engineered so as to approximate the delay that would be experienced with the use of a comparable geometric optic. If similar techniques were to be scaled to terahertz frequencies then this would provide high spectral bandwidth. Additional to that, all-dielectric reflector devices of low dispersion have previously been demonstrated in the terahertz range [86], and hence this presents a potential avenue of exploration for the development of low-dispersion terahertz reflectarray antennas.

At a more fundamental level, an issue that affects reflectarray antennas at all frequency ranges is inter-resonator coupling between heterogeneous elements. As previously mentioned in Section II-C, this can impact the validity of unit cell analysis in describing the behavior of a given resonator when deployed in the reflectarray. However, the assumption of local periodicity, in conjunction with unit cell analysis, is presently the norm in reflectarray design. This approach gives accurate results in cases in which the phase varies gradually across the array surface, but validity decreases in those cases in which the phase variation presents abrupt jumps [87]–[89]. As such, reflectarray antennas in general can benefit significantly from approaches to modeling that account for coupling in a nonuniform array. A straightforward example of such a procedure is the manual adjustment of metallic resonator dimensions described in Section IV. Note, this process of manual optimization is not general, and would not be applicable to less straightforward, non-periodic phase distributions. However, a related approach has previously been employed for a lensing transmitarray in the optical range [90], in which relevant portions of the array are decomposed into a radial arrangement of what are essentially deflector sub-arrays, which can be optimized in a way that incorporates coupling effects. Alternatively, rapid advances in computational power would be instrumental for optimizing complete arrays, with coupling effects fully incorporated.

VII. Conclusion

We have presented a summary of our recent work on terahertz reflectarray antennas, consisting of the design, fabrication, and experimental characterization of four different reflectarray devices. We have contrasted metallic resonator and DRA-based approaches, demonstrating three examples of the former, and one of the latter. In general, metallic resonators offer a higher degree of choice and control over polarization-sensitive functionality, but DRAs offer far greater efficiency. The devices presented in this work can be adapted to produce terahertz antennas with diverse characteristics, including high antenna gain, polarization sensitivity, and customizable radiation patterns. It is anticipated that, with advances in terahertz resonator technology, dynamic steerability will become a reality, which would likely propel applications including short-range terahertz communications into the domain of commercial viability.

Acknowledgment

The authors wish to thank C. Shah, A. Upadhyay, S. Nirantar, and P. Gutruf for carrying out the microfabrication of the devices presented in this paper.

References

[1] H.-J. Song and T. Nagatsuma, "Present and future of terahertz communications," *IEEE Trans. THz Sci. Technol.*, vol. 1, no. 1, pp. 256–263, Sep. 2011.
[2] T. Kleine-Ostmann and T. Nagatsuma, "A review on terahertz communications research," *J. Infrared, Millim., THz Waves*, vol. 32, no. 2, pp. 143–171, 2011.
[3] T. Nagatsuma, G. Ducournau, and C. C. Renaud, "Advances in terahertz communications accelerated by photonics," *Nature Photon.*, vol. 10, no. 6, pp. 371–379, 2016.
[4] C. B. Reid *et al.*, "Accuracy and resolution of THz reflection spectroscopy for medical imaging," *Phys. Med. Biol.*, vol. 55, no. 16, pp. 4825–4838, 2010.
[5] C. Yu, S. Fan, Y. Sun, and E. Pickwell-MacPherson, "The potential of terahertz imaging for cancer diagnosis: A review of investigations to date," *Quant. Imaging Med. Surg.*, vol. 2, no. 1, pp. 33–45, 2012.
[6] A. Luukanen, R. Appleby, M. Kemp, and N. Salmon, "Millimeter-wave and terahertz imaging in security applications," in *Terahertz Spectroscopy and Imaging*. New York, NY, USA: Springer, 2013, pp. 491–520.
[7] J. Chamberlain, "Where optics meets electronics: Recent progress in decreasing the terahertz gap," *Philos. Trans. Roy. Soc. A*, vol. 362, no. 1815, pp. 199–213, 2004.
[8] D. M. Mittleman, "Frontiers in terahertz sources and plasmonics," *Nature Photon.*, vol. 7, no. 9, pp. 666–669, 2013.
[9] *Attenuation by Atmospheric Gases*. International Telecommunication Union ITU-R Recommendation P.676-10, 2013.
[10] J. Huang and J. A. Encinar, *Reflectarray Antennas*. New York, NY, USA: Wiley, 2008.
[11] E. Carrasco, M. Barba, and J. A. Encinar, "Reflectarray element based on aperture-coupled patches with slots and lines of variable length," *IEEE Trans. Antennas Propag.*, vol. 55, no. 3, pp. 820–825, Mar. 2007.
[12] S. M. A. M. H. Abadi, K. Ghaemi, and N. Behdad, "Ultra-wideband, true-time-delay reflectarray antennas using ground-plane-backed, miniaturized-element frequency selective surfaces," *IEEE Trans. Antennas Propag.*, vol. 63, no. 2, pp. 534–542, Feb. 2015.
[13] D. Berry, R. Malech, and W. Kennedy, "The reflectarray antenna," *IEEE Trans. Antennas Propag.*, vol. AP-11, no. 6, pp. 645–651, Nov. 1963.
[14] C. Malagisi, "Microstrip disc element reflect array," in *Proc. Electron. Aerosp. Syst. Conv.*, 1978, vol. 1, pp. 186–192.
[15] D. M. Pozar, S. D. Targonski, and H. Syrigos, "Design of millimeter wave microstrip reflectarrays," *IEEE Trans. Antennas Propag.*, vol. 45, no. 2, pp. 287–296, Feb. 1997.
[16] A. Ahmadi, S. Ghadarghadr, and H. Mosallaei, "An optical reflectarray nanoantenna: The concept and design," *Opt. Express*, vol. 18, no. 1, pp. 123–133, 2010.
[17] L. Zou *et al.*, "Dielectric resonator nanoantennas at visible frequencies," *Opt. Express*, vol. 21, no. 1, pp. 1344–1352, 2013.
[18] L. Zou *et al.*, "Spectral and angular characteristics of dielectric resonator metasurface at optical frequencies," *Appl. Phys. Lett.*, vol. 105, no. 19, 2014, Art. no. 191109.

[19] Y. Yang *et al.*, "Dielectric meta-reflectarray for broadband linear polarization conversion and optical vortex generation," *Nano Lett.*, vol. 14, no. 3, pp. 1394–1399, 2014.

[20] H. Hasani, *et al.*, "Tri-band, polarization-independent reflectarray at terahertz frequencies: Design, fabrication,and measurement," *IEEE Trans. THz Sci. Technol.*, vol. 6, no. 2, pp. 268–277, Mar. 2016.

[21] C. G. Ryan *et al.*, "A wideband transmitarray using dual-resonant double square rings," *IEEE Trans. Antennas Propag.*, vol. 58, no. 5, pp. 1486–1493, May 2010.

[22] F. Monticone, N. M. Estakhri, and A. Alù, "Full control of nanoscale optical transmission with a composite metascreen," *Phys. Rev. Lett.*, vol. 110, no. 20, 2013, Art. no. 203903.

[23] X. Zhang *et al.*, "Broadband terahertz wave deflection based on C-shape complex metamaterials with phase discontinuities," *Adv. Mater.*, vol. 25, no. 33, pp. 4567–4572, 2013.

[24] D. R. Smith, W. J. Padilla, D. Vier, S. C. Nemat-Nasser, and S. Schultz, "Composite medium with simultaneously negative permeability and permittivity," *Phys. Rev. Lett.*, vol. 84, no. 18, pp. 4184–4187, 2000.

[25] D. R. Smith, D. Vier, N. Kroll, and S. Schultz, "Direct calculation of permeability and permittivity for a left-handed metamaterial," *Appl. Phys. Lett.*, vol. 77, no. 14, pp. 2246–2248, 2000.

[26] W. Withayachumnankul and D. Abbott, "Metamaterials in the terahertz regime," *IEEE Photon. J.*, vol. 1, no. 2, pp. 99–118, Aug. 2009.

[27] E. F. Kuester, M. A. Mohamed, M. Piket-May, and C. L. Holloway, "Averaged transition conditions for electromagnetic fields at a metafilm," *IEEE Trans. Antennas Propag.*, vol. 51, no. 10, pp. 2641–2651, Oct. 2003.

[28] C. L. Holloway, M. A. Mohamed, E. F. Kuester, and A. Dienstfrey, "Reflection and transmission properties of a metafilm: With an application to a controllable surface composed of resonant particles," *IEEE Trans. Electromagn. Compat.*, vol. 47, no. 4, pp. 853–865, Nov. 2005.

[29] M. F. Volk, B. Reinhard, J. Neu, R. Beigang, and M. Rahm, "In-plane focusing of terahertz surface waves on a gradient index metamaterial film," *Opt. Lett.*, vol. 38, no. 12, pp. 2156–2158, 2013.

[30] N. Chamok, M. Ali, T. Anthony, and S. J. Weiss, "Ultra-thin UHF broadband antenna on a non-uniform aperiodic (NUA) metasurface," *IEEE Antennas Propag. Mag.*, vol. 57, no. 2, pp. 167–180, Apr. 2015.

[31] N. Yu *et al.*, "Light propagation with phase discontinuities: Generalized laws of reflection and refraction," *Science*, vol. 334, no. 6054, pp. 333–337, 2011.

[32] N. K. Grady *et al.*, "Terahertz metamaterials for linear polarization conversion and anomalous refraction," *Science*, vol. 340, no. 6138, pp. 1304–1307, 2013.

[33] R. Bansal, "Bending Snell's laws," *IEEE Ant. Propag. Mag.*, vol. 53, no. 5, pp. 146–147, Oct. 2011.

[34] S. Larouche and D. R. Smith, "Reconciliation of generalized refraction with diffraction theory," *Opt. Lett.*, vol. 37, no. 12, pp. 2391–2393, Jun. 2012.

[35] E. Carrasco, M. Barba, and J. A. Encinar, "X-band reflectarray antenna with switching-beam using pin diodes and gathered elements," *IEEE Trans. Antennas Propag.*, vol. 60, no. 12, pp. 5700–5708, Dec. 2012.

[36] G. Perez-Palomino, J. Encinar, R. Dickie, and R. Cahill, "Preliminary design of a liquid crystal-based reflectarray antenna for beam-scanning in THz," in *Proc. IEEE Antennas Propag. Soc. Int. Symp.*, 2013, pp. 2277–2278.

[37] E. Carrasco, M. Tamagnone, J. R. Mosig, T. Low, and J. Perruisseau-Carrier, "Gate-controlled mid-infrared light bending with aperiodic graphene nanoribbons array," *Nanotechnology*, vol. 26, no. 13, 2015, Art. no. 134002.

[38] S. C. Saha, C. Li, Y. Ma, J. P. Grant, and D. R. S. Cumming, "Fabrication of multilevel silicon diffractive lens at terahertz frequency," *IEEE Trans. THz Sci. Technol.*, vol. 3, no. 4, pp. 479–485, Jul. 2013.

[39] D. Headland *et al.*, "Analysis of 3D-printed metal for rapid-prototyped reflective terahertz optics," *Opt. Express*, vol. 24, no. 15, pp. 17 384–17 396, Jul. 2016.

[40] T. Niu *et al.*, "Experimental demonstration of reflectarray antennas at terahertz frequencies," *Opt. Express*, vol. 21, no. 3, pp. 2875–2889, 2013.

[41] T. Niu *et al.*, "Terahertz reflectarray as a polarizing beam splitter," *Opt. Express*, vol. 22, no. 13, pp. 16 148–16 160, 2014.

[42] T. Niu *et al.*, "Polarization-dependent thin-film wire-grid reflectarray for terahertz waves," *Appl. Phys. Lett.*, vol. 107, no. 3, 2015, Art. no. 031111.

[43] D. Headland *et al.*, "Dielectric resonator reflectarray as high-efficiency non-uniform terahertz metasurface," *ACS Photon.*, vol. 3, no. 6, pp. 1019–1026, 2016.

[44] C. A. Balanis, *Antenna Theory: Analysis and Design*, 4th ed. New York, NY, USA: Wiley, 2016.

[45] D.-W. Duan and Y. Rahmat-Samii, "A generalized diffraction synthesis technique for high performance reflector antennas," *IEEE Trans. Antennas Propag.*, vol. 43, no. 1, pp. 27–40, Jan. 1995.

[46] F. J. Villegas, "Parallel genetic-algorithm optimization of shaped beam coverage areas using planar 2-D phased arrays," *IEEE Trans. Antennas Propag.*, vol. 55, no. 6, pp. 1745–1753, Jun. 2007.

[47] D. Pozar, S. Targonski, and R. Pokuls, "A shaped-beam microstrip patch reflectarray," *IEEE Trans. Antennas Propag.*, vol. 47, no. 7, pp. 1167–1173, Jul. 1999.

[48] J. A. Encinar and J. A. Zornoza, "Three-layer printed reflectarrays for contoured beam space applications," *IEEE Trans. Antennas Propag.*, vol. 52, no. 5, pp. 1138–1148, May 2004.

[49] J. A. Encinar *et al.*, "Dual-polarization dual-coverage reflectarray for space applications," *IEEE Trans. Antennas Propag.*, vol. 54, no. 10, pp. 2827–2837, Oct. 2006.

[50] J. W. Goodman, *Introduction to Fourier Optics*. Greenwood Village, CO, USA: Roberts and Company Publ., 2005.

[51] R. W. Gerchberg and W. O. Saxton, "A practical algorithm for the determination of phase from image and diffraction plane pictures," *Optik*, vol. 35, pp. 237–246, 1972.

[52] V. Lomakin, Y. Fainman, Y. Urzhumov, and G. Shvets, "Doubly negative metamaterials in the near infrared and visible regimes based on thin film nanocomposites," *Opt. Express*, vol. 14, no. 23, pp. 11164–11177, 2006.

[53] C. Qu *et al.*, "Tailor the functionalities of metasurfaces based on a complete phase diagram," *Phys. Rev. Lett.*, vol. 115, no. 23, 2015, Art. no. 235503.

[54] D. F. Sievenpiper, J. H. Schaffner, H. J. Song, R. Y. Loo, and G. Tangonan, "Two-dimensional beam steering using an electrically tunable impedance surface," *IEEE Trans. Antennas. Propag.*, vol. 51, no. 10, pp. 2713–2722, Oct. 2003.

[55] R. Singh *et al.*, "Observing metamaterial induced transparency in individual fano resonators with broken symmetry," *Appl. Phys. Lett.*, vol. 99, no. 20, 2011, Art. no. 201107.

[56] Y. Z. Cheng *et al.*, "Ultrabroadband reflective polarization convertor for terahertz waves," *Appl. Phys. Lett.*, vol. 105, no. 18, 2014, Art. no. 181111.

[57] D. Headland *et al.*, "Terahertz magnetic mirror realized with dielectric resonator antennas," *Adv. Mater.*, vol. 27, no. 44, pp. 7137–7144, 2015.

[58] P. Drude, "Zur Elektronentheorie der Metalle," *Ann. Phys.*, vol. 306, no. 3, pp. 566–613, 1900.

[59] S. Walia *et al.*, "Flexible metasurfaces and metamaterials: A review of materials and fabrication processes at micro-and nano-scales," *Appl. Phys. Rev.*, vol. 2, no. 1, 2015, Art. no. 011303.

[60] N. Laman and D. Grischkowsky, "Terahertz conductivity of thin metal films," *Appl. Phys. Lett.*, vol. 93, no. 5, 2008, Art. no. 051105.

[61] S. Wang *et al.*, "Experimental verification of negative refraction for a wedge-type negative index metamaterial operating at terahertz," *Appl. Phys. Lett.*, vol. 97, no. 18, 2010, Art. no. 181902.

[62] A. Ebrahimi *et al.*, "Second-order terahertz bandpass frequency selective surface with miniaturized elements," *IEEE Trans. THz Sci. Technol.*, vol. 5, no. 5, pp. 761–769, Sep. 2015.

[63] N. Jukam and M. S. Sherwin, "Two-dimensional terahertz photonic crystals fabricated by deep reactive ion etching in Si," *Appl. Phys. Lett.*, vol. 83, no. 1, pp. 21–23, 2003.

[64] J.-X. Zhuang, Z.-C. Hao, and W. Hong, "Silicon micromachined terahertz bandpass filter with elliptic cavities," *IEEE Trans. THz Sci. Technol.*, vol. 5, no. 6, pp. 1040–1047, Nov. 2015.

[65] Y. Z. Cheng *et al.*, "Ultrabroadband plasmonic absorber for terahertz waves," *Adv. Opt. Mater.*, vol. 3, no. 3, pp. 376–380, 2015.

[66] I. Khodasevych *et al.*, "Elastomeric silicone substrates for terahertz fishnet metamaterials," *Appl. Phys. Lett.*, vol. 100, no. 6, 2012, Art. no. 061101.

[67] J. Dai, J. Zhang, W. Zhang, and D. Grischkowsky, "Terahertz time-domain spectroscopy characterization of the far-infrared absorption and index of refraction of high-resistivity, float-zone silicon," *J. Opt. Soc. Am. B*, vol. 21, no. 7, pp. 1379–1386, 2004.

[68] T. Niu, W. Withayachumnankul, and C. Fumeaux, "Terahertz reflectarray for bidirectional beam splitting," in *Proc. 39th Int. Conf. Infrared, Millim., THz Waves*, 2014, pp. 1–2, doi: 10.1109/IRMMW-THz.2014.6956410.

[69] H. Tao *et al.*, "Terahertz metamaterials on free-standing highly-flexible polyimide substrates," *J. Phys. D, Appl. Phys.*, vol. 41, no. 23, 2008, Art. no. 232004.

[70] S. A. Long, M. W. McAllister, and L. C. Shen, "The resonant cylindrical dielectric cavity antenna," *IEEE Trans. Antennas Propag.*, vol. 31, no. 3, pp. 406–412, May 1983.

[71] L. Zou *et al.*, "Efficiency and scalability of dielectric resonator antennas at optical frequencies," *IEEE Photon. J.*, vol. 6, no. 4, 2014, Art. no. 4600110.

[72] W. Withayachumnankul, B. M. Fischer, H. Lin, and D. Abbott, "Uncertainty in terahertz time-domain spectroscopy measurement," *J. Opt. Soc. Am. B*, vol. 25, no. 6, pp. 1059–1072, 2008.
[73] W. Withayachumnankul, J. F. O'Hara, W. Cao, I. Al-Naib, and W. Zhang, "Limitation in thin-film sensing with transmission-mode terahertz time-domain spectroscopy," *Opt. Express*, vol. 22, no. 1, pp. 972–986, 2014.
[74] A. P. Feresidis, G. Goussetis, S. Wang, and J. C. Vardaxoglou, "Artificial magnetic conductor surfaces and their application to low-profile high-gain planar antennas," *IEEE Trans. Antennas. Propag.*, vol. 53, no. 1, pp. 209–215, Jan. 2005.
[75] C. Guclu, J. Sloan, S. Pan, and F. Capolino, "Direct use of the high impedance surface as an antenna without dipole on top," *IEEE Antennas Wireless Propag. Lett.*, vol. 10, pp. 1536–1539, Dec. 2011.
[76] A. Vallecchi, J. R. De Luis, F. Capolino, and F. De Flaviis, "Low profile fully planar folded dipole antenna on a high impedance surface," *IEEE Trans. Antennas. Propag.*, vol. 60, no. 1, pp. 51–62, Jan. 2012.
[77] Y. Monnai *et al.*, "Terahertz beam steering and variable focusing using programmable diffraction gratings," *Opt. Express*, vol. 21, no. 2, pp. 2347–2354, 2013.
[78] K. Sengupta and A. Hajimiri, "A 0.28 THz power-generation and beam-steering array in CMOS based on distributed active radiators," *IEEE J. Solid-State Circuits*, vol. 47, no. 12, pp. 3013–3031, Dec. 2012.
[79] G. Sharma *et al.*, "Carrier density dependence of the nonlinear absorption of intense THz radiation in GaAs," *Opt. Express*, vol. 20, no. 16, pp. 18016–18024, 2012.
[80] I. Al-Naib *et al.*, "Effect of local field enhancement on the nonlinear terahertz response of a silicon-based metamaterial," *Phys. Rev. B*, vol. 88, no. 19, 2013, Art. no. 195203.
[81] E. Carrasco, M. Tamagnone, and J. Perruisseau-Carrier, "Tunable graphene reflective cells for THz reflectarrays and generalized law of reflection," *Appl. Phys. Lett.*, vol. 102, 2013, Art. no. 104103.
[82] E. Carrasco and J. Perruisseau-Carrier, "Reflectarray antenna at terahertz using graphene," *IEEE Antennas Wireless Propag. Lett.*, vol. 12, pp. 253–256, Feb. 2013.
[83] M. Tamagnone *et al.*, "Near optimal graphene terahertz non-reciprocal isolator," *Nature Commun.*, vol. 7, 2016, Art. no. 11216.
[84] B. Jin *et al.*, "Low loss and magnetic field-tunable superconducting terahertz metamaterial," *Opt. Express*, vol. 18, no. 16, pp. 17504–17509, 2010.
[85] E. Carrasco, J. A. Encinar, and M. Barba, "Bandwidth improvement in large reflectarrays by using true-time delay," *IEEE Trans. Antennas Propag.*, vol. 56, no. 8, pp. 2496–2503, Aug. 2008.
[86] I. A. Ibraheem, N. Krumbholz, D. Mittleman, and M. Koch, "Low-dispersive dielectric mirrors for future wireless terahertz communication systems," *IEEE Microw. Compon. Lett.*, vol. 18, no. 1, pp. 67–69, Jan. 2008.
[87] E. Carrasco *et al.*, "Design, manufacture and test of a low-cost shaped-beam reflectarray using a single layer of varying-sized printed dipoles," *IEEE Trans. Antennas Propag.*, vol. 61, no. 6, pp. 3077–3085, Jun. 2013.
[88] M. Zhou *et al.*, "The generalized direct optimization technique for printed reflectarrays," *IEEE Trans. Antennas Propag.*, vol. 62, no. 4, pp. 1690–1700, Apr. 2014.
[89] R. Florencio, R. R. Boix, and J. A. Encinar, "Fast and accurate mom analysis of periodic arrays of multilayered stacked rectangular patches with application to the design of reflectarray antennas," *IEEE Trans. Antennas Propag.*, vol. 63, no. 6, pp. 2558–2571, Jun. 2015.
[90] S. J. Byrnes, A. Lenef, F. Aieta, and F. Capasso, "Designing large, high-efficiency, high-numerical-aperture, transmissive meta-lenses for visible light," *Opt. Express*, vol. 24, no. 5, pp. 5110–5124, 2016.

Daniel Headland (S'14–M'16) received the B.Eng. (first class hons.) from The University of Adelaide, Adelaide, SA, Australia, in 2012. He commenced his doctoral program at The University of Adelaide in 2013, having attained the George Fraser Scholarship, which is awarded to the highest ranking Ph.D. applicant for that year.

His research interests include terahertz technology, wavefront engineering, terahertz and submillimeter-wave antennas, and electromagnetics.

Tiaoming Niu received the B.S. and M.S. degrees from Lanzhou University, Lanzhou, China, in 2003 and 2011, respectively, and the Ph.D. degree in electrical engineering from The University of Adelaide, Adelaide, SA, Australia, in 2015.

She is currently a Lecturer of the School of Information Science and Engineering, Lanzhou University, Lanzhou, China. Her research interests include terahertz technology, metamaterials, and reflectarray antennas.

Eduardo Carrasco (S'96–M'08) received the Telecommunication Engineering degree from the National Autonomous University of Mexico, Mexico City, Mexico, in 2000, and the Telecommunication Engineering Ph.D. degree from the Technical University of Madrid (UPM), Madrid, Spain, in 2008.

From 1999 to 2001, he was with Directv Latin America as Broadcast Operation System Specialist. In 2002, he received a grant from Fundacion Vodafone, Spain, to obtain a Telecommunication Management Degree in the School for Industrial Organization, Spain. From January to April 2008, he visited the Microwave Engineering Laboratory, University of Perugia, Perugia, Italy, as part of the Ph.D. research work. From June 2009 to June 2012, he was with the Electromagnetism and Circuit Theory Department, UPM, Spain, as a Postdoctoral Researcher, participating in different projects supported by the Spanish Government, the Mexican Council of Science and Technology, the European Union's Sixth and Seventh Framework Programs (FP6 & FP7), and the European Space Agency. From 2012 to 2014, he was with the Adaptive Micronano Wave Systems Group, Swiss Federal Institute of Technology, Lausanne, Switzerland, as a Marie-Curie Fellow. From January 2015, he took up a position as Electromagnetic Simulation, Dosimetry, and Antenna Engineer at the Foundation for Research on Information Technologies in Society, Zurich, Switzerland. His main interests include planar antenna arrays, reconfigurable antenna arrays, as well as EMF exposure limits and compliance, and oncological hyperthermia treatment planning. He is a member of the Mexican Network of Space Science and Technology, the European Association on Antennas and Propagation, and the Institute of Electrical and Electronics Engineers.

Derek Abbott (M'85–SM'99–F'05) was born in South Kensington, London, U.K., in 1960. He received the B.Sc. (Hons.) degree in physics from Loughborough University, Leicestershire, U.K., in 1982 and the Ph.D. degree in electrical and electronic engineering from The University of Adelaide, Adelaide, SA, Australia, in 1995, under K. Eshraghian and B. R. Davis.

From 1978 to 1986, he was a Research Engineer with the GEC Hirst Research Centre, London, U.K. From 1986 to 1987, he was a VLSI Design Engineer with Austek Microsystems, Australia. Since 1987, he has been with The University of Adelaide, where he is currently a Full Professor with the School of Electrical and Electronic Engineering. He has authored or coauthored more than 800 publications and a number of patents. His research interests include multidisciplinary physics and electronic engineering applied to complex systems, networks, game theory, energy policy, stochastics, and biophotonics.

Prof. Abbott has been an invited speaker at more than 100 institutions. He coedited *Quantum Aspects of Life* (Imperial College Press, 2008), and coauthored *Stochastic Resonance* (Cambridge Univ. Press, 2008) and *Terahertz Imaging for Biomedical Applications* (Springer-Verlag, 2012). He is a Fellow of the Institute of Physics. He has been an Editor and/or Guest Editor for a number of journals, including the IEEE JOURNAL OF SOLID-STATE CUIRCUITS, *Journal of Optics B*, *Microelectronics Journal*, *PLOSONE*, PROCEEDINGS OF THE IEEE, and the IEEE PHOTONICS JOURNAL. He is currently on the Editorial Boards of IEEE ACCESS, Natures *Scientific Reports*, *Royal Society Open Science*, and *Frontiers in Physics*.

Prof. Abbott received a number of awards, including the Tall Poppy Award for Science (2004), the Premiers SA Great Award in Science and Technology for outstanding contributions to South Australia (2004), an Australian Research Council Future Fellowship (2012), and the David Dewhurst Medal (2015).

Sharath Sriram (S'04–M'09) received the Ph.D. degree from RMIT University, Melbourne, VIC, Australia, in 2009.

He is the joint leader of the Functional Materials and Microsystems Research Group, RMIT University, Melbourne, Australia. He is also the Scientific Coordinator of the University's Micro Nano Research Facility, a 1200 m^2 state-of-the-art micro/nanofabrication capability. His expertise includes the synthesis of functional thin films and micro/nanostructures and devices. He has published more than 120 peer-reviewed publications. He received the 2010 Gold Medal for Excellence in Research from the Australian Institute of Nuclear Science and Engineering, a 2011–2014 Australian Post-Doctoral Fellowship from the Australian Research Council, the 2012 NMI Prize for Measurement Excellence from the National Measurement Institute, Australia, a 2012 Victoria Fellowship, the 2014 RMIT Vice-Chancellor's Early Career Researcher Award, and the 2016 Australian Museum 3M Eureka Prize for Emerging Leader in Science.

Madhu Bhaskaran (S'04–M'09) received the Ph.D. degree from RMIT University, Melbourne, VIC, Australia, in 2009.

She jointly leads the Functional Materials and Microsystems Research Group, RMIT University, Australia. Her research interests include stretchable electronics, functional oxides, and micro/nanoelectronics. She has published more than 85 peer-reviewed journal articles. She received a 2010–2014 Australian Post-Doctoral Fellowship from the Australian Research Council, the 2011 RMIT Vice-Chancellor's Early Career Researcher Award, the 2011 RMIT Media Star Award for Research, the 2014 Phillip Law Post-Doctoral Award for Physical Sciences awarded by the Royal Society of Victoria, a 2016–2018 Australian Research Council early-career fellowship, and was named as one of the Top 10 Innovators Under 35 in Asia in 2015 by the MIT Technology Review.

Christophe Fumeaux (M'03–SM'09) received the Diploma and Ph.D. degrees in physics from the ETH Zurich, Zurich, Switzerland, in 1992 and 1997, respectively. From 1998 to 2000, he was a Postdoctoral Researcher with the School of Optics, University of Central Florida, Orlando, FL, USA. In 2000, he joined the Swiss Federal Office of Metrology as a Scientific Staff Member. From 2001 to 2008, he was a Research Associate and Group Leader with the Laboratory for Electromagnetic Fields and Microwave Electronics at ETH Zurich. Since 2008, he has been with The University of Adelaide, Adelaide, SA, Australia, where he is currently a Professor with the School of Electrical and Electronic Engineering. His current main research interests concern computational electromagnetics, antenna engineering, terahertz technology and the application of RF design principles to optical micro/nanostructures.

Prof. Fumeaux has served as an Associate Editor for the IEEE TRANSACTIONS ON MICROWAVE THEORY AND TECHNIQUES from 2010 to 2013. From 2013 to 2016, he has been serving as Senior Associate Editor and later Associate Editor-in-Chief for the IEEE TRANSACTIONS ON ANTENNAS AND PROPAGATION. He received the ETH Silver Medal of Excellence for his doctoral dissertation. From 2011 to 2015, he was a Future Fellow of the Australian Research Council. He was the recipient/co-recipient of best journal paper awards, including the 2004 *ACES Journal* and 2014 IEEE SENSORS JOURNAL, as well as best conference paper awards at the 2012 Asia-Pacific International Symposium on Electromagnetic Compatibility (APEMC 2012) and the 17th Colloque International sur la Compatibilité Electromagnétique (CEM 2014). Several of his students have received student awards with joint papers, including IMS 2006 & 2007, iWAT 2014, AMS 2014, IEEE Australia Council 2014, NEMO 2015, and ICEAA 2015 & 2016.

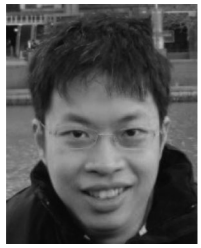

Withawat Withayachumnankul (SM'16) received the B.Eng. and M.Eng. degrees in electronic engineering from King Mongkut's Institute of Technology Ladkrabang (KMITL), Bangkok, Thailand, in 2001 and 2003, and the Ph.D. degree in electrical engineering (with commendation) from the University of Adelaide, Adelaide, SA, Australia, in 2010. From 2003 to 2012, he served as a Lecturer at KMITL with the Faculty of Engineering. From 2010 to 2013, he held an ARC Australian Postdoctoral Fellowship with the University of Adelaide, and has been a Lecturer there since 2014. In 2015, he was a Research Fellow of the Japan Society for the Promotion of Science at the Tokyo Institute of Technology. His research interests include terahertz technology, metamaterials, plasmonics, and optical antennas.

Dr. Withayachumnankul has authored and coauthored more than 58 journal publications. He has delivered invited talks at ETH Zürich, University of Marburg, Universität Kaiserslautern, EPFL, Nanyang Technological University, Nagoya University, Keio University, and Osaka University, among other institutes. He serves as a Grant Assessor for Swiss National Science Foundation, German Academic Exchange Service, French Agence Nationale de la Recherche, and Australian Research Council. He received the IEEE/LEOS Graduate Student Fellowship (2008) and the SPIE Scholarship in Optical Science and Engineering (2008).